9, and 12 months. Patients seen at the National Institutes of Health Clinical Center returned their bottles of medication, and pill counts were performed. Nearly all of these patients had an excellent rate of compliance with the study medication. Of 56 subjects, 45 completed the study. Five subjects were excluded from analysis due to insufficient peripheral blood mononuclear cells (PBMCs) available for all five time points or no detectable EBV DNA in the blood at any time point throughout the study. All other subjects had measurable levels of EBV DNA for at least three different time points, including day 0.

Isolation of DNA from B cells and real-time PCR. PBMCs were isolated from whole blood and stored in liquid nitrogen. For each subject, samples from each time point were thawed and processed at the same time. B cells were isolated by negative selection (human B-cell isolation kit; Miltenyi Biotec, Germany), resuspended in 100 to 200 μl of phosphate-buffered saline, and counted. Preliminary experiments showed no notable inhibition of the real-time PCR with fewer than 10^4 cells but mild to modest inhibition with more than 5×10^4 cells/well. Therefore, the concentration of cells was adjusted to 4,000 cells per 5 μl (some experiments used 1,500 to 8,000 cells per 5 μl), and 5 μl of B cells was plated into wells of a 96-well real-time PCR plate and stored at −20°C. For all specimens, a small portion of leftover cell suspension was stained with anti-CD20 monoclonal antibody conjugated with phycoerythrin (BD Pharmingen, San Diego, CA), and the purity of B cells was determined by flow cytometry. In most experiments, the fraction of B cells in each cell suspension was >80%. All plates from the same subject were thawed at the same time, and 5 μl of buffer containing proteinase K and Tween 20 was added to each well to disrupt cells as previously described (13). Quantitative real-time PCR amplification was performed by adding 15 μl of PCR master mix (Eurogentec North America, San Diego, CA) containing EBV BamHI W primers and probes (12) to each well of B-cell DNA. The limit of detection using this PCR system is ~4 copies per reaction, based on experiments using standard curves obtained with serial dilutions of a plasmid with a single copy of BamHI W. Since EBV genomes contain 5 to 12 copies of BamHI W repeats (1) and each infected cell contains at least one EBV genome, this system has the potential to detect a single EBV-infected cell per well. Since we did not know the number of BamHI W repeats for each patient's virus, we expressed the data as the number of EBV DNA copies per infected cell. We compared each patient to him- or herself over time, and the number of copies of BamHI W repeats per viral genome is not likely to change in a given patient.

Calculations to determine the number of EBV-infected cells and average EBV genome copy number per infected cell. In the real-time PCR plates, most wells were negative for EBV DNA because of the low frequency of EBV-infected cells in healthy subjects. The number of positive wells depended on the frequency of EBV-positive B cells, the purity of B cells, and the number of cells applied to each well. Since the number of EBV-positive B cells per well was very low, we used a Poisson distribution to calculate this number (as we previously described for calculating the number of HSV-positive cells per well [13]). We defined the total number of wells in the plate as n and the number of EBV-positive wells as y. We assume that the number of EBV-infected cells per well follows a Poisson distribution with parameter a. Assuming a Poisson distribution for the number of EBV-positive cells within a well, the probability that a well has at least one positive cell is $1 - e^{-a}$ (where e is the base of the natural logarithm). Thus, an estimate of a is obtained by equating the observed proportion of positive wells, or y/n, to $1 - e^{-a}$. Solving this equation for a gives $a = -\ln(1 - y/n)$. For plates without any positive wells, i.e., $y = 0$, this estimate is 0 regardless of the value for the number of total wells (n). However, plates with many wells have a more reliable 0 than plates with few wells. We thus smoothed the data to address this issue and pretended that each plate had one additional well that was 0.5 positive and estimated a as follows: $a = -\ln[1 - (y + 0.5)/(n + 1)]$. Instead of estimating the proportion of positive wells by the ratio y/n, we used $(y + 0.5)/(n + 1)$, which is the Bayesian posterior mean of the proportion of negative wells under a Jeffreys noninformative prior (5). Therefore, the estimation of the number of EBV-positive cells/well is as follows: $a = -\ln[1 - (y + 0.5)/(n + 1)]$. This can be viewed loosely as the "middle" of a confidence interval for the true proportion of positive wells. This smoothing method gives modestly higher estimates for plates with positive wells and has values closer to zero for totally negative plates with many wells compared to totally negative plates with few wells.

We can also estimate the frequency of a B cell being infected by EBV as follows: $q = a/(m \times p/100)$, where m is the number of cells per well and p is the purity of B cells (%). We thus estimate q as follows: $q = a/(m \times p/100) = -\ln[1 - (y + 0.5)/(n + 1)]/(m \times p/100)$. To estimate the average number of EBV DNA copies per infected cell, the sum of all EBV genomes in a plate (S) was determined directly from real-time PCR results and was divided by an estimate of the number of EBV-positive B cells in the plate ($a \times n$). For example, if a plate contained three EBV-positive wells, with 110, 58, and 152 EBV copies, S equaled 320. See Table 1 for an example.

TABLE 1. Sensitivity of real-time PCR assay

No. of X50-7 cells/well	Total no. of wells	No. of EBV-positive wells	Observed frequency of EBV-positive wells[a]	Predicted frequency of EBV-positive wells[b]	No. of EBV DNA copies/infected cell[c]
0.00	16	0	0.00	0.00	NA
0.25	24	3	0.13	0.22	19.3
1.00	24	12	0.50	0.63	28.4
4.00	24	23	0.96	0.98	18.9

[a] Observed frequency of EBV-positive wells = number of EBV-positive wells (third column) divided by total number of wells (second column).

[b] Predicted frequencies of EBV-positive wells were calculated from the Poisson distribution (see text for details).

[c] Calculation of the number of EBV DNA copies/infected cell is described in Table 2, footnote *c*, and in the text. NA, not applicable.

RESULTS

Development of a technique to estimate the frequency of EBV-positive cells and the average number of EBV DNA copies/B cell in healthy persons. We initially tried to determine the number of EBV DNA copies in B cells isolated from PBMCs by using real-time PCR, but we found that viral loads in healthy individuals were too low to detect in a reproducible fashion; therefore, we used a novel approach involving quantification of the EBV DNA copy number using limiting dilution of B cells and real-time PCR, similar to the approach previously described for quantifying HSV DNA in ganglion cells (13). This method allowed us to estimate both the frequency of EBV-positive B cells and the average number of copies of EBV genomes per EBV-infected cell.

We initially tested the sensitivity of the assay using an EBV cell line, X50-7, with a known number of copies of EBV DNA per cell (2). Serial fourfold dilutions of X50-7 cells (beginning at four cells per well) were added to EBV-negative BJAB cells (4,000 BJAB cells/well), and the number of EBV-positive wells and number of EBV DNA copies per infected cell were determined. The observed frequency of EBV-positive wells for each dilution was similar to the predicted frequency based on the Poisson distribution, and the average number of EBV DNA copies per EBV-positive X50-7 cell for each dilution was consistent (Table 1). Based on the Poisson distribution, the probability that any well contained two or more EBV-positive cells when EBV-positive cells were plated at a concentration of 0.25 cells per well was 2.6% $[(1 - 1.25\ e^{-0.25}) \times 100]$. Therefore, we expected only 1 EBV-positive cell per well when the cells were plated at a concentration of 0.25 EBV-positive cells/well. Since we were able to detect EBV DNA in some wells with an average of 0.25 EBV-positive cells per well, our real-time PCR system was able to detect single EBV-positive cells in a well.

We next tested blood bank donors for EBV-positive B cells and EBV DNA copy numbers, using the assay. For blood bank donor A, 8 of 56 wells were positive for EBV DNA (Table 2, columns 2 and 3), and we estimated the number of EBV-positive cells/well as follows: $a = -\ln[1 - (8 + 0.5)/(56 + 1)] = 0.161$ (Table 2, column 4 and footnote *a*). Based on the estimate of the number of EBV-positive cells/well (0.161), the number of cells added to each well (2,500), and the purity of the B cells (87.9%) (Table 2, columns 4, 5, and 6, respectively, and footnote *a*), there was an estimated $(0.161 \times 10^7)/(2{,}500 \times 87.9) = 7.35$ EBV-positive cells/10^5 B cells (Table 2, column 7

TABLE 2. Estimation of numbers of EBV-infected B cells and EBV DNA copies per infected cell in blood bank donors

Donor	Total no. of wells (n)	No. of EBV-positive wells (y)	Estimation of no. of EBV-positive cells/well[a] (a)	No. of cells added to well (m)	Purity of B cells (%) (p)	No. of EBV-positive cells/10^5 B cells[b] (q)	Sum of EBV DNA copies (S)	No. of EBV DNA copies/infected cell[c]
A	56	8	0.161	2,500	87.9	7.35	2,062	229
	32	9	0.340	3,000	94.5	11.98	1,432	132
B	44	2	0.057	3,500	95.6	1.71	449	179
	88	8	0.100	4,000	96.4	2.60	1,003	114
C	88	38	0.567	4,000	83.5	16.96	3,583	71.8
	38	14	0.465	4,000	76.2	15.25	2,168	123
D	44	18	0.530	3,310	94.0	17.02	3,136	135
	44	13	0.357	3,430	92.4	11.25	1,909	122
	88	34	0.491	3,570	92.4	14.87	2,354	123
	85	29	0.420	3,620	89.7	12.94	1,317	66
	88	50	0.838	4,000	94.3	22.22	3,862	114

[a] Estimation of number of EBV-positive cells/well, $a = -\ln|1 - (y + 0.5)/(n + 1)|$, where n is the total number of wells in the plate (second column) and y is the number of EBV-positive wells (third column).

[b] The number of EBV-positive cells/10^5 B cells, $q = (a \times 10^7)/(m \times p)$, where a is the estimation of the number of EBV-positive cells/well (fourth column), m is the number of cells in a well (fifth column), and p is the percent purity of B cells (sixth column). Each well contains $(m \times p)/100$ B cells.

[c] The number of EBV DNA copies/infected cell = $S/(a \times n)$, where S is the sum of all EBV genome numbers from a plate (eighth column; obtained directly from real-time PCR results), a is the estimation of the number of EBV-positive cells/well (fourth column), and n is the number of wells in the plate (second column). Therefore, $(a \times n)$ is the number of EBV-positive cells in the plate.

and footnote *b*). Using the total number of wells (56), the estimate of the number of EBV-positive cells/well (0.161), and the sum of EBV DNA copies in the plate (2,062) (Table 2, columns 2, 4, and 8, respectively), there was an average of 2,062/(0.161 × 56) = 229 EBV DNA copies/infected B cell (Table 2, column 9 and footnote *c*), since our primers and probe for real-time PCR detect each copy of the BamHI W repeat. In a second experiment using cells from the same donor drawn on the same day, 9 of 32 wells were positive for EBV, with an estimated 11.98 EBV-positive cells/10^5 B cells and an average of 132 EBV DNA copies/infected B cell. In experiments with cells from blood bank donors B, C, and D, the numbers of EBV-infected B cells and copies of EBV DNA per B cell were similar for a given donor from the same day in independent experiments, with different numbers of wells and purities of B cells (Table 2). The mean number (± standard deviation) of EBV-positive cells per 10^5 B cells for donors A, B, C, and D was 9.7 ± 3.3, 2.2 ± 0.6, 16.1 ± 1.2, and 15.7 ± 4.3, respectively. The mean number (± standard deviation) of EBV DNA copies per infected cell for donors A, B, C, and D was 181 ± 69, 147 ± 46, 97 ± 36, and 112 ± 27, respectively. Thus, this method provides an estimation of the frequency of EBV-positive cells and the average number of EBV DNA copies/B cell at low viral loads with reasonable reproducibility.

The number of EBV-infected B cells declines during valacyclovir treatment in healthy persons. Using this approach, we determined the number of EBV-infected B cells and the average number of EBV DNA copies per infected cell for patients receiving valacyclovir or no antiviral therapy in the clinical study. There were 21 subjects in the control group and 19 subjects in the valacyclovir group. We analyzed the rate of change in the number of EBV-infected cells for each subject over time, since a large variation in the number of EBV-infected B cells between subjects could underestimate the difference in the change in virus-infected cells. The number of EBV-positive cells per 10^5 B cells was plotted against time, in months, for the first three patients enrolled in each group (Fig. 1). While there was variation during the five time points, we were able to plot a linear regression line for each subject. We then determined linear regression lines and slopes for the number of EBV-positive cells per 10^5 B cells over time for all of the subjects in the study (Fig. 2; data used to generate regression lines are shown in the supplemental material). There was considerable variability in the starting value (*y* intercept) of each line as well as in the slope of the regression line among subjects even within the same group. The average of the regression lines (thick gray lines in Fig. 2A) was relatively flat for the control group but had a negative slope for the valacyclovir group. The mean of the slopes for the valacyclovir-treated group was $-2.8 \times 10^{-2} \pm 1.2 \times 10^{-2}$/month and was statistically different from a slope of 0 ($P = 0.02$), while the mean of the slopes for the control group was $-0.1 \times 10^{-2} \pm 0.8 \times 10^{-2}$/month, which was not statistically different from 0

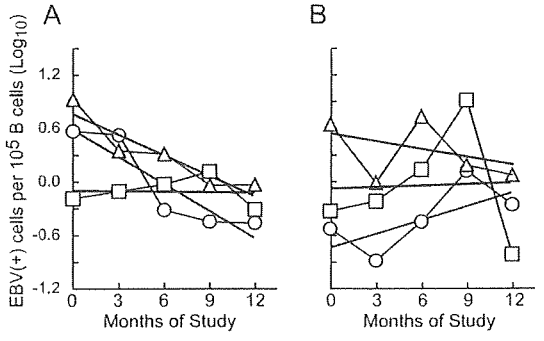

FIG. 1. EBV-positive cells per 10^5 B cells over time and linear regression lines for the first three subjects from the valacyclovir (A) and control (B) groups. Each symbol connected with a broken line represents data for one subject. Solid lines associated with symbols indicate linear regression lines of the data for each subject.

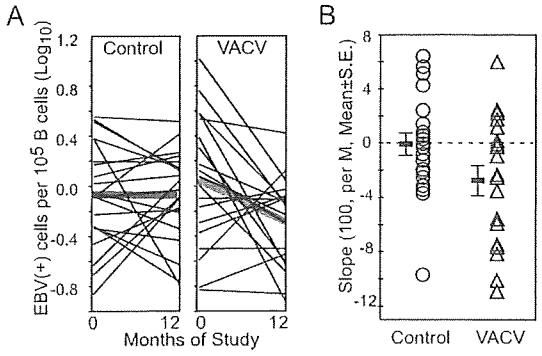

FIG. 2. Rate of change (slope) in the number of EBV-infected B cells over time. (A) Linear regression lines for individual control subjects (left) and valacyclovir (VACV) patients (right) are shown as thin lines. Thick gray lines indicate the mean slope for each group. (B) The individual slopes for each control subject (circles) and valacyclovir patient (triangles) are depicted. Short horizontal bars indicate means, and vertical bars indicate standard errors (S.E.).

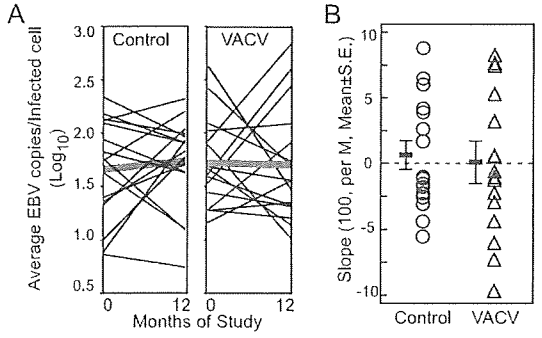

FIG. 3. Mean EBV DNA copies per B cell over time. (A) Linear regression lines for individual control subjects (left) and valacyclovir (VACV) patients (right) are shown as thin lines. Thick gray lines indicate the mean slope for each group. (B) The individual slopes for each control subject (circles) and valacyclovir patient (triangles) are depicted. Short horizontal bars indicate means, and vertical bars indicate standard errors (S.E.).

($P = 0.86$) (Fig. 2B). Comparison of the slopes of regression lines between the two treatment groups showed that the difference approached statistical significance ($P = 0.054$; Wilcoxon test). The slopes of the control and valacyclovir groups were significantly different using regression analysis, with the viral load ($\log_{10}$) as outcome and month as the covariate ($P = 0.03$ for common delta), and when analyzed using analysis of covariance, with slope as outcome and intercept as the covariate ($P = 0.04$ for common delta). These findings indicate that the number of EBV-infected B cells declined over time in the valacyclovir treatment group.

The EBV DNA copy number per infected B cell does not decline during valacyclovir treatment in healthy persons. We next examined the effect of valacyclovir treatment on the number of EBV DNA copies per infected cell. The mean number (± standard error) of EBV DNA copies per infected B cell was 64.0 ± 17.1 for patients in the valacyclovir group and 67.9 ± 15.4 for patients in the control group. The slopes of linear regression lines for the mean number of EBV DNA copies per infected cell over time (in months) were determined for each subject (Fig. 3A), and the mean slopes for the two groups were compared (Fig. 3B). The mean regression lines had slopes of nearly 0 for both groups. The slopes of the rate of change in the number of EBV DNA copies per infected cell over time for both the control and the valacyclovir groups were indistinguishable from 0 ($P = 0.62$ and $P = 0.92$ for the control and valacyclovir groups, respectively), and the difference in mean slopes between the groups was not significant ($P = 0.66$). Thus, the mean EBV DNA copy number per infected cell ($\log_{10}$) is stable over time and is not affected by 1 year of valacyclovir therapy.

DISCUSSION

We have shown that 1 year of valacyclovir therapy in healthy EBV carriers results in a decrease in the number of EBV-infected B cells compared to an untreated control group, while valacyclovir has no effect on the mean number of EBV DNA copies per infected cell. The somewhat modest effect in the reduction of EBV load after 1 year of valacyclovir was not unexpected. Acyclovir inhibits EBV lytic replication, which uses the viral DNA polymerase in B cells, but has no effect on EBV replication in latently infected B cells, which uses the host cell polymerase. The increase in the frequency of EBV-infected cells in five of the subjects receiving valacyclovir suggests that these persons may have had proliferation of B cells latently infected with EBV (and insensitive to valacyclovir); alternatively, they may have been noncompliant with the antiviral medication. The observation that 28 days of acyclovir had no effect on the EBV load (23) suggested that a more prolonged course of antiviral therapy was likely to have only a modest effect in reducing the viral load.

The half-life of EBV-infected cells during convalescence after infectious mononucleosis (~6 weeks from first visit) was reported to be 7.5 ± 3.7 days (11). Since EBV is latent in memory B cells, which have a half-life of 11 ± 3.3 days (17), Hadinoto et al. proposed a model for the decline of EBV-infected B cells after mononucleosis based on the kinetics of turnover of memory B cells (11). From our data, the half-life of EBV-infected B cells in the valacyclovir group based on the mean slopes ($-2.8 \times 10^{-2} \pm 1.2 \times 10^{-2}$/month) was 11 months, and the half-life calculated from median slopes was 12 months. In the control group, the half-life of EBV-infected B cells calculated from mean slopes ($-0.1 \times 10^{-2} \pm 0.8 \times 10^{-2}$/month) was 31 years, and that calculated from the median slopes was 41 years. There are several possibilities that may explain the discrepancy between our results and those of the prior study. First, Hadinoto et al. (11) measured the half-life of EBV in the blood during convalescence from mononucleosis, whereas our subjects presumably had been infected many years earlier. Balfour and colleagues (3) and Fafi-Kremer et al. (9) showed that the level of EBV in PBMCs was still elevated 6 weeks after primary infection. Second, one dose of valacyclovir each day is unlikely to completely block EBV reactivation and virus production. While the bioavailability of valacyclovir is about three to five times higher than that of acyclovir, valacyclovir is converted into acyclovir in the body, and the mean plasma elimination time of acyclovir is 1.5 to 6.3 h (4, 15). Third, it is possible that latent infection of memory B cells with

EBV prolongs the half-life of these cells or that EBV may establish latency preferentially in a subset of memory B cells that has a longer life span. Fourth, compared with EBV-infected B cells from patients convalescing after infectious mononucleosis, EBV-infected B cells in our subjects might be more heterogeneous, with some infected cells resting, others actively proliferating, and a small minority undergoing lytic replication. Since valacyclovir affects only lytic replication of EBV, the marked differences in the decline of EBV copy numbers in different valacyclovir recipients (Fig. 2) might reflect differences in the relative proportions of resting, proliferating, and lytically infected cells. Nonetheless, the general reduction of EBV-infected B cells over time in the valacyclovir group suggests that infection by EBV of previously uninfected B cells is one of the mechanisms that maintains the latent EBV pool in healthy adults.

EBV can be eliminated from the body in some patients after bone marrow transplantation (10). Based on the half-life of EBV in patients treated with valacyclovir and assuming that valacyclovir acts similarly on B cells in tissues as it does in the blood, we estimate that it would take 6 years of 500 mg of valacyclovir once each day to eradicate 99% of EBV from the B-cell compartment and 11.3 years to eliminate the virus completely from the body if persons were not reinfected during this time. Reinfection with the virus is likely, however, since multiple strains of EBV are detected in many individuals, suggesting that multiple episodes of infection occur (22). The mean peak concentration of acyclovir reaches 27.1 μM when valacyclovir is given at 1,000 mg three times a day (16), while the 50% effective inhibitory dose of acyclovir for EBV replication is 5 to 10 μM (7, 21, 24). Therefore, it might be theoretically possible to eradicate EBV from the body within several years with high-dose valacyclovir. Acyclovir or valacyclovir prophylaxis has been reported to have various rates of effectiveness in reducing the risk of EBV lymphoproliferative disease in transplant recipients (8, 18). The relatively modest effect of valacyclovir in reducing EBV DNA in B cells in the blood after a full year in persons with a healthy immune system suggests that more active drugs against EBV might be more effective for prophylaxis of EBV lymphoproliferative disease in immunocompromised persons.

ACKNOWLEDGMENTS

This study was supported by the intramural research program of the National Institute of Allergy and Infectious Diseases.

We dedicate this paper to the memory of Stephen Straus, whose commitment to patients with Epstein-Barr virus diseases inspired our work.

REFERENCES

1. **Allan, G. J., and D. T. Rowe.** 1989. Size and stability of the Epstein-Barr virus major internal repeat (IR-1) in Burkitt's lymphoma and lymphoblastoid cell lines. Virology **173**:489–498.
2. **Arribas, J. R., D. B. Clifford, C. J. Fichtenbaum, R. L. Roberts, W. G. Powderly, and G. A. Storch.** 1995. Detection of Epstein-Barr virus DNA in cerebrospinal fluid for diagnosis of AIDS-related central nervous system lymphoma. J. Clin. Microbiol. **33**:1580–1583.
3. **Balfour, H. H., Jr., C. J. Holman, K. M. Hokanson, M. M. Lelonek, J. E. Giesbrecht, D. R. White, D. O. Schmeling, C. H. Webb, W. Cavert, D. H. Wang, and R. C. Brundage.** 2005. A prospective clinical study of Epstein-Barr virus and host interactions during acute infectious mononucleosis. J. Infect. Dis. **192**:1505–1512.
4. **Blum, M. R., S. H. Liao, and P. de Miranda.** 1982. Overview of acyclovir pharmacokinetic disposition in adults and children. Am. J. Med. **73**:186–192.
5. **Brown, L. D., T. T. Cai, and A. DasGupta.** 2001. Interval estimation for a binomial proportion. Stat. Sci. **16**:101–133.
6. **Cohen, J. I.** 2000. Epstein-Barr virus infection. N. Engl. J. Med. **343**:481–492.
7. **Colby, B. M., J. E. Shaw, G. B. Elion, and J. S. Pagano.** 1980. Effect of acyclovir [9-(2-hydroxyethoxymethyl)guanine] on Epstein-Barr virus DNA replication. J. Virol. **34**:560–568.
8. **Darenkov, I. A., M. A. Marcarelli, G. P. Basadonna, A. L. Friedman, K. M. Lorber, J. G. Howe, J. Crouch, M. J. Bia, A. S. Kliger, and M. I. Lorber.** 1997. Reduced incidence of Epstein-Barr virus-associated posttransplant lymphoproliferative disorder using preemptive antiviral therapy. Transplantation **64**:848–852.
9. **Fafi-Kremer, S., P. Morand, J. P. Brion, P. Pavese, M. Baccard, R. Germi, O. Genoulaz, S. Nicod, M. Jolivet, R. W. Ruigrok, J. P. Stahl, and J. M. Seigneurin.** 2005. Long-term shedding of infectious Epstein-Barr virus after infectious mononucleosis. J. Infect. Dis. **191**:985–989.
10. **Gratama, J. W., M. A. Oosterveer, J. M. Lepoutre, J. J. van Rood, F. E. Zwaan, J. M. Vossen, J. G. Kapsenberg, D. Richel, G. Klein, and I. Ernberg.** 1990. Serological and molecular studies of Epstein-Barr virus infection in allogeneic marrow graft recipients. Transplantation **49**:725–730.
11. **Hadinoto, V., M. Shapiro, T. C. Greenough, J. L. Sullivan, K. Luzuriaga, and D. A. Thorley-Lawson.** 2008. On the dynamics of acute EBV infection and the pathogenesis of infectious mononucleosis. Blood **111**:1420–1427.
12. **Hoover, S. E., J. Kawada, W. Wilson, and J. I. Cohen.** 2008. Oropharyngeal shedding of Epstein-Barr virus in the absence of circulating B cells. J. Infect. Dis. **198**:318–323.
13. **Hoshino, Y., J. Qin, D. Follmann, J. I. Cohen, and S. E. Straus.** 2008. The number of herpes simplex virus-infected neurons and the number of viral genome copies per neuron correlate with the latent viral load in ganglia. Virology **372**:56–63.
14. **Khan, G., E. M. Miyashita, B. Yang, G. J. Babcock, and D. A. Thorley-Lawson.** 1996. Is EBV persistence in vivo a model for B cell homeostasis? Immunity **5**:173–179.
15. **Laskin, O. L.** 1983. Clinical pharmacokinetics of acyclovir. Clin. Pharmacokinet. **8**:187–201.
16. **Lycke, J., C. Malmestrom, and L. Stahle.** 2003. Acyclovir levels in serum and cerebrospinal fluid after oral administration of valacyclovir. Antimicrob. Agents Chemother. **47**:2438–2441.
17. **Macallan, D. C., D. L. Wallace, Y. Zhang, H. Ghattas, B. Asquith, C. de Lara, A. Worth, G. Panayiotakopoulos, G. E. Griffin, D. F. Tough, and P. C. Beverley.** 2005. B-cell kinetics in humans: rapid turnover of peripheral blood memory cells. Blood **105**:3633–3640.
18. **McDiarmid, S. V., S. Jordan, G. S. Kim, M. Toyoda, J. A. Goss, J. H. Vargas, M. G. Martin, R. Bahar, A. L. Maxfield, M. E. Ament, and R. W. Busuttil.** 1998. Prevention and preemptive therapy of postransplant lymphoproliferative disease in pediatric liver recipients. Transplantation **66**:1604–1611.
19. **Miyashita, E. M., B. Yang, K. M. Lam, D. H. Crawford, and D. A. Thorley-Lawson.** 1995. A novel form of Epstein-Barr virus latency in normal B cells in vivo. Cell **80**:593–601.
20. **Oyama, T., K. Yamamoto, N. Asano, A. Oshiro, R. Suzuki, Y. Kagami, Y. Morishima, K. Takeuchi, T. Izumo, S. Mori, K. Ohshima, J. Suzumiya, N. Nakamura, M. Abe, K. Ichimura, Y. Sato, T. Yoshino, T. Naoe, Y. Shimoyama, Y. Kamiya, T. Kinoshita, and S. Nakamura.** 2007. Age-related EBV-associated B-cell lymphoproliferative disorders constitute a distinct clinicopathologic group: a study of 96 patients. Clin. Cancer Res. **13**:5124–5132.
21. **Pagano, J. S., and A. K. Datta.** 1982. Perspectives on interactions of acyclovir with Epstein-Barr and other herpes viruses. Am. J. Med. **73**:18–26.
22. **Tierney, R. J., R. H. Edwards, D. Sitki-Green, D. Croom-Carter, S. Roy, Q. Y. Yao, N. Raab-Traub, and A. B. Rickinson.** 2006. Multiple Epstein-Barr virus strains in patients with infectious mononucleosis: comparison of ex vivo samples with in vitro isolates by use of heteroduplex tracking assays. J. Infect. Dis. **193**:287–297.
23. **Yao, Q. Y., P. Ogan, M. Rowe, M. Wood, and A. B. Rickinson.** 1989. Epstein-Barr virus-infected B cells persist in the circulation of acyclovir-treated virus carriers. Int. J. Cancer **43**:67–71.
24. **Zacny, V. L., E. Gershburg, M. G. Davis, K. K. Biron, and J. S. Pagano.** 1999. Inhibition of Epstein-Barr virus replication by a benzimidazole L-riboside: novel antiviral mechanism of 5,6-dichloro-2-(isopropylamino)-1-beta-L-ribofuranosyl-1H-benzimidazole. J. Virol. **73**:7271–7277.

Journal of Medical Virology 81:1951–1958 (2009)

Detection of Merkel Cell Polyomavirus in Merkel Cell Carcinoma and Kaposi's Sarcoma

Harutaka Katano,[1]* Hideki Ito,[2] Yoshio Suzuki,[3] Tomoyuki Nakamura,[1] Yuko Sato,[1] Takahiro Tsuji,[1] Koma Matsuo,[2] Hidemi Nakagawa,[2] and Tetsutaro Sata[1]

[1]*Department of Pathology, National Institute of Infectious Diseases, Shinjuku, Tokyo, Japan*
[2]*Department of Dermatology, Jikei University School of Medicine, Minato, Tokyo, Japan*
[3]*Department of Pathology, Asahi General Hospital, Asahi, Chiba, Japan*

Merkel cell carcinoma is a rare malignancy that sometimes occurs in the skin of elderly people. Recently, a new human polyomavirus, Merkel cell polyomavirus (MCPyV) was identified in Merkel cell carcinoma. In the present study, MCPyV-DNA was detected in 6 of 11 (55%) cases of Merkel cell carcinoma by nested PCR and real-time PCR. Histologically, MCPyV-positive cases showed round and vesicular nuclei with a fine granular chromatin and small nucleoli, whereas MCPyV-negative cases showed polygonal nuclei with diffusely distributed chromatin. Real-time PCR analysis to detect the MCPyV gene revealed that viral copy numbers ranged 0.04–0.43 per cell in cases of Merkel cell carcinoma. MCPyV was also detected in 3 of 49 (6.1%) cases of Kaposi's sarcoma (KS), but not in 192 DNA samples of other diseases including 142 autopsy samples from 20 immunodeficient patients. The MCPyV copy number in KS was lower than that in Merkel cell carcinoma. PCR successfully amplified a full-length MCPyV genome from a case of KS. Sequence analysis revealed that the MCPyV isolated from KS had 98% homology to the previously reported MCPyV genomes. These data suggest that the prevalence of MCPyV is low in Japan, and is at least partly associated with the pathogenesis of Merkel cell carcinoma. ***J. Med. Virol. 81:1951–1958, 2009.***

KEY WORDS: Merkel cell polyomavirus; Merkel cell carcinoma; real-time PCR; Kaposi's sarcoma

INTRODUCTION

Merkel cell carcinoma is a rare skin malignancy that originates in the Merkel cell, a neuroendocrine cell in the skin [Skelton et al., 1997; Pectasides et al., 2006; Lemos and Nghiem, 2007]. Merkel cell carcinoma is an aggressive skin cancer that commonly occurs on sun-exposed areas of elderly people. The incidence of Merkel cell carcinoma is high in Caucasians, but lower in other races [Agelli and Clegg, 2003]. Typical histology of Merkel cell carcinoma shows that the tumor consists of small, round cells with vesicular nuclei, fine chromatin, and minimal cytoplasm. Because these morphological features are similar to other small cell tumors such as small cell lung cancer and lymphoma, immunohistochemistry for cytokeratin 20 is often useful for differential diagnosis. Recurrence and metastasis in the regional lymph nodes are observed in up to 30% of cases [Agelli and Clegg, 2003]. Merkel cell carcinoma comprises two subtypes, "classic" and "variant," based on clinical manifestations and gene expression profiles [Van Gele et al., 2004; Fernandez-Figueras et al., 2007]. Gene expression profiling studies have also demonstrated that metastasis of Merkel cell carcinoma is correlated with the over-expression of some metastasis-associated proteins such as matrix metalloproteinases [Fernandez-Figueras et al., 2007].

A new human polyomavirus, Merkel cell polyomavirus (MCPyV), was identified recently in samples of Merkel cell carcinoma by digital transcriptome subtraction [Feng et al., 2008]. MCPyV is a 5.4-kbp long, double-stranded DNA virus and has high

Grant sponsor: Health and Labor Sciences Research Grants from the Ministry of Health, Labor and Welfare; Grant numbers: H21-AIDS-Ippan-006 (partial support to H.K.), H19-AIDS-Ippan-003 (to H.K.); H20-Nanchi-Ippan-035 (to T.S.); H20-Shinko-Ippan-006 (to T.S.); Grant sponsor: Ministry of Education, Culture, Sports, Science and Technology of Japan (to H.K.); Grant number: 21590520; Grant sponsor: Research on Health Sciences Focusing on Drug Innovation from the Japan Health Sciences Foundation (to H.K. and T.S.); Grant number: SAA4832.

*Correspondence to: Harutaka Katano, Department of Pathology, National Institute of Infectious Diseases, 1-23-1 Toyama, Shinjuku, Tokyo 162-8640, Japan. E-mail: katano@nih.go.jp

Accepted 29 June 2009
DOI 10.1002/jmv.21608
Published online in Wiley InterScience (www.interscience.wiley.com)

homology to murine, African green monkey, and hamster polyomaviruses. The MCPyV genome encodes a large T antigen, which contains some conserved domains that were shown previously to play roles in cell transformation. In an earlier report, MCPyV was detected in 8 out of 10 cases of Merkel cell carcinoma (80%) by PCR, and clonal integration into the human genome was observed in 6 of the 8 cases with Merkel cell carcinoma [Feng et al., 2008]. Several recent reports have demonstrated the presence of MCPyV in Merkel cell carcinoma cases in the United States, Europe, and Australia, but is rare in other samples such as melanoma, skin cancer, other cancers, and controls [Foulongne et al., 2008; Giraud et al., 2008; Kassem et al., 2008; Becker et al., 2009; Bialasiewicz et al., 2009; Bluemn et al., 2009; Duncavage et al., 2009; Garneski et al., 2009; Goh et al., 2009; Ridd et al., 2009; Sharp et al., 2009]. A study using frozen samples of Merkel cell carcinoma demonstrated that all Merkel cell carcinoma samples were positive for MCPyV-DNA [Sastre-Garau et al., 2009]. These data strongly suggest that MCPyV infection is associated with the pathogenesis of Merkel cell carcinoma [zur Hausen, 2008]. On the other hand, studies using paraffin-embedded tissues suggest the presence of some MCPyV-negative cases of Merkel cell carcinoma [Foulongne et al., 2008; Kassem et al., 2008; Becker et al., 2009; Duncavage et al., 2009; Garneski et al., 2009]. In addition, MCPyV is less frequently present in Merkel cell carcinoma in Australian cases than in North American cases, suggesting geographic differences of MCPyV distribution [Garneski et al., 2009]. Although there are no accurate statistical data, Merkel cell carcinoma seems to be rare in Japan. In this study, the presence of MCPyV was investigated in Japanese cases of Merkel cell carcinoma and other diseases.

MATERIALS AND METHODS

Specimens

Studies using human tissue were performed with the approval of the Institutional Review Board of the National Institute of Infectious Diseases (Approval No. 149). Thirteen formalin-fixed paraffin-embedded tissue samples of Merkel cell carcinoma were collected from 11 patients (Table I). All of the samples were taken by biopsy or from tumor resection, and were enriched in tumor cells. The diagnosis of Merkel cell carcinoma was based on morphology and immunohistochemistry of cytokeratin 20. In addition to the Merkel cell carcinoma samples, 49 DNA samples of Kaposi's sarcoma (KS) and 50 DNA samples from tissues with various diseases were collected. A further 142 DNA samples were extracted from various organs of 20 autopsy cases with AIDS. All these human samples were archived as anonymous specimens held at the Department of Pathology, National Institute of Infectious Diseases. DNA extracted from 15 cell lines was also investigated.

TABLE I. MCPyV Infection in Merkel Cell Carcinoma Cases

Clinical information				Nested PCR for MCPyV						Real-time PCR		
Case	Sex	Age	Site	ST	LT (1017–1170)	LT (2057–2107)	VP1	VP2	VP3	MCPyV copy per 100 ng DNA	β-Actin copy per 100 ng DNA	Predicted MCPyV copy per cell
1	F	89	Cheek	−	−	−	−	−	−	0	17,505	0.000
2	F	104	Cheek	+	+	+	+	+	+	356	1,645	0.433
3	F	76	Forearm	+	+	−	−	−	−	247	12,980	0.038
4	F	50	Face	+	+	+	+	+	+	617	7,300	0.169
5	M	87	Face	−	−	−	−	−	−	0	2,053	0.000
6	M	90	Head	−	−	−	−	−	−	0	670	0.000
7	F	89	Face	−	−	−	−	−	−	0	11,940	0.000
8	F	95	Inguinal	−	−	−	−	−	−	0	39,865	0.000
8*	F	95	Abdomen	−	−	−	−	−	−	0	13,520	0.000
9	F	86	Face	+	+	+	+	+	+	691	18,960	0.073
9*	F	86	Face	+	+	−	+	+	+	78	2,796	0.056
10	M	78	Forearm	+	+	−	+	+	+	93	911	0.206
11	F	96	Cheek	+	+	−	+	−	−	50	423	0.119

Samples 8* and 9* are recurrent tumors of cases 8 and 9, respectively.

Preparation of DNA

DNA was extracted from formalin-fixed paraffin-embedded or fresh-frozen clinical materials. To isolate DNA from formalin-fixed paraffin-embedded biopsies, 5-μm-thick sections (n = 3–4) were placed into sterile eppendorf tubes, deparaffinized with xylene, digested with proteinase K, and processed for phenol/chloroform extraction with sodium acetate/ethanol precipitation. For fresh-frozen materials, DNeasy Tissue Kit (Qiagen GmbH, Hilden, Germany) was used according to the manufacturer's instructions.

Nested PCR

The small T (ST), large T (LT), and VP1–3 regions of MCPyV were amplified by nested PCR. The primer sequences are listed in Table II. The first round of amplification was performed with 100 ng of extracted DNA and high fidelity Taq DNA polymerase (Roche Diagnostics, Boehringer Mannheim, Germany) in a final volume of 25 μl. After an initial DNA denaturation for 2 min at 94°C, the samples were amplified for 35 cycles of 94°C for 30 sec, 55°C for 30 sec, and 72°C for 30 sec, followed by a final elongation phase of 7 min at 72°C. The second round of amplification was performed with 1 μl of the first round PCR product in a final volume of 25 μl under the following parameters: 94°C for 30 sec, 55°C for 30 sec, 72°C for 30 sec for 25 cycles, followed by a final elongation phase of 7 min at 72°C. Five microliters of amplification products were loaded onto agarose gels, electrophoresed, stained with bromide and visualized under UV light. The β-globin gene was amplified as an internal control by single PCR [Katano et al., 2001].

DNA Sequencing

The PCR products from nested PCR were sequenced directly with an ABI sequencer 3730 (Applied Biosystems, Foster City, CA) using a dye terminator ready reaction kit (Applied Biosystems) according to the manufacturer's instructions.

Real-Time PCR

Copy numbers of MCPyV-DNA were determined by quantitative real-time TaqMan PCR using the Mx3005P real-time PCR system (Stratagene, La Jolla, CA), which amplified a segment within the LT (1017–1170) domain. The amount of human genomic DNA (β-actin gene) present in the DNA extracted from each specimen was also determined. Primers and probes for the MCPyV-LT gene were designed using Primer Express software (Applied Biosystems). To amplify MCPyV-LT, forward (Merkel PV LT Forward: 5′-TCTGGGTATGGGTCCTT-CTCA-3′) and reverse (Merkel PV LT Reverse: 5′-TGG-TGTTCGGGAGGTATATCG-3′) primers were used with a labeled probe 5′-(FAM)CGTCCCAGGCTTCAGACTC-CCAGTC(TAMRA)-3′. To amplify β-actin DNA, forward (5′-TGAGCGCGGCTACAGCTT-3′) and reverse (5′-TC-CTTAATGTCACGCACGATTT-3′) primers were used with a labeled probe 5′-(FAM)ACCACCACGGCCGAG-CGG(TAMRA)-3′ [Kuramochi et al., 2006]. The amplicon sizes of MCPyV-LT and β-actin were 77 bp (1053–1129 in GenBank EU375803) and 60 bp (655–714 in NM_001101), respectively. PCR amplification was performed in 20-μl reaction mixtures using QuantiTect probe PCR Master Mix (Qiagen), 0.3 μM of each primer, 0.3 μM of TaqMan probe, and 2 μl isolated

TABLE II. Primers Used for Nested PCR

Gene	Out/in	F/r	Primer name	5′–3′	Position*	Size (bp)
ST	Outer	Forward	MCV-ST-F515	CTGGGTGCATGCTTAAGCAAC	515–732	218
		Reverse	MCV-ST-R732	GCAGTAGTCAGTTTCTTCT		
	Inner	Forward	MCV-ST-F550	TGCGCTTGTATTAGCTGTAAGT	550–703	154
		Reverse	MCV-ST-R703	GCCACCAGTCAAAACTTTCCCA		
LT (1017–1170)	Outer	Forward	MCV-LT-F992	CTCCAATGCATCCAGGGGAG	992–1192	201
		Reverse	MCV-LT-R1192	TCTCTTCCTGAATTGGTGGT		
	Inner	Forward	MCV-LT-F1017	AGTGGAAGCTCACCACCCCACA	1017–1170	154
		Reverse	MCV-LT-R1170	CCTCTCTGCTACTGGATCCA		
LT (2057–2207)	Outer	Forward	MCV-LT-F2034	CCATTTCCTTGCCAAAAGTG	2034–2228	195
		Reverse	MCV-LT-R2228	CTTACATAGCATTTCTGTCC		
	Inner	Forward	MCV-LT-F2057	AAACAGATCTCGCCTCAAAC	2057–2207	150
		Reverse	MCV-LT-R2207	GGTCATTTCCAGCATCTCTA		
VP1	Outer	Forward	MCV-VP1-F4233	TGAATCCAAGAATGGGAGTT	4062–4252	191
		Reverse	MCV-VP1-R4062	CATCTGCAATGTGTCACAG		
	Inner	Forward	MCV-VP1-F4212	TCCCCTGATCTTCCTACT	4092–4229	138
		Reverse	MCV-VP1-R4092	ATTTAGCATTGGCAGAGAC		
VP2	Outer	Forward	MCV-VP2-F4490	CAATCTGGAGTTTGCTGCTG	4490–4692	203
		Reverse	MCV-VP2-R4692	CTGCATTCTGTGGGGCAAAAT		
	Inner	Forward	MCV-VP2-F4511	AGAGTTCCTCCTATATGTTC	4511–4661	151
		Reverse	MCV-VP2-R4661	TTTATCTCCTACCTCTAGGC		
VP3	Outer	Forward	MCV-VP3-F4890	CCAAAGAAGCCACTAATGAG	4890–5118	229
		Reverse	MCV-VP3-R5118	ATGGGGGGCATCATCACACTG		
	Inner	Forward	MCV-VP3-F4932	TGAACCCAAGTTGAGCTAAAGC	4932–5097	166
		Reverse	MCV-VP3-R5097	CTGGCCAATATTGGTGAAATTG		

*Position in GenBank EU375803.

DNA. The PCR conditions were: 95°C for 15 min, followed by 40 cycles of 94°C for 15 sec and 60°C for 1 min. Quantitative results were obtained by generating standard curves for pCR2.1 plasmids (Invitrogen, Carlsbad, CA) containing each MCPyV-LT and the cellular target (β-actin gene) amplicon. Virus copy numbers per cell were calculated by dividing MCPyV-LT copy numbers by half of the β-actin copy numbers, because each cell contains two copies of DNA in two alleles [Asahi-Ozaki et al., 2006].

Histological and Immunohistochemical Analyses

Immunohistochemistry was performed to investigate the expression of cytokeratin 20, chromogranin and neuron-specific enolase (NSE) on paraffin-embedded tissues of Merkel cell carcinoma. Sections (4 μm thick) were deparaffinized by sequential immersion in xylene and ethanol, and rehydrated in distilled water. For antigen retrieval, the sections were autoclaved in 1 mM EDTA, 0.05 M Tris–HCl, pH 9.0, at 121°C for 10 min for cytokeratin 20 and chromogranin, or 0.01 M citrate buffer at 95°C for 10 min for NSE. Endogenous peroxidase activity was blocked by immersing the sections in methanol/0.6% H_2O_2 for 30 min at room temperature. Diluted anti-cytokeratin 20 (Dako, Copenhagen, Denmark), chromogranin (Dako), or NSE (Novocastra Laboratories, Newcastle, UK) antibodies were applied and the sections were incubated overnight at 4°C. After washing in PBS twice, a biotinyl anti-mouse IgG goat antibody and peroxidase-conjugated streptavidin were used as the secondary and tertiary antibodies, respectively. 3,3′-diaminobenzidine was used as a chromogen.

Cloning of a Full-Length MCPyV Genome

A full-length MCPyV genome was amplified by single PCR using KOD-FX DNA polymerase (Toyobo, Tokyo, Japan) according to the manufacturer's instructions. A primer-set (primer set 1: MCV-*Bam*HI-1150F TCTGGATCCAGTAGCAGAGAGGAGACC and MCV-*Bam*HI-1150R CTCGGATCCAGAGGATGAGGTGGGTTC) was used to amplify the full-length MCV genome. Following the addition of dA to the PCR product, the PCR product was TA-cloned into pCR2.1 vector (Invitrogen). Primer set 2 (MCV-F133 CTTAGTGAGGTAGCTCATTTGCTCCTCTGCTGTT and MCV-R5325 AACTTTTATTGCTGCAGGGTTTCTGGCATTGACTC) was used to amplify almost the full-length of the MCPyV genome except for the origin region. A 1,188-bp-fragment containing the origin region was amplified using another primer set (primer set 3: MCV-VP3-F4932 TGAACCCAAGTTGAGCTAAAGC and MCV-ST-R732 GCAGTAGTCAGTTTCTTCT).

RESULTS

PCR Detection of MCPyV in Merkel Cell Carcinoma

To determine whether MCPyV is present in Japanese cases of Merkel cell carcinoma, PCR analysis was first performed on DNA samples extracted from 11 cases of Merkel cell carcinoma using primers specific for the MCPyV-LT and VP1 regions, as published previously [Feng et al., 2008]. Although the β-globin gene was amplified in all DNA samples, fragments of MCPyV were not detected using these primers (data not shown). Thus, nested PCR, which can detect gene fragments <250 bp in length, was performed for six MCPyV genes (Table II). Nested PCR revealed that 6 of the 11 Merkel cell carcinoma cases (54.5%) were positive for MCPyV ST and LT (1017–1170) fragments (Fig. 1 and Table I). Interestingly, LT (2057–2107) and VP2-3 were detected in cases 2, 4, and 9, but not in cases 3, 10, or 11. LT (2057–2107) was not detected in the recurrent samples of case 9. Sequencing analysis revealed that all these PCR products were fragments of MCPyV, and an A to G mutation was detected at the position 4589 of GenBank EU375803 in the VP2 fragments of cases 2, 4, 9, and 10 with Merkel cell carcinoma. In addition, two mutations, G4996C and A5032T, were detected in the VP3 fragments of cases 2, 4, 9, and 10, which were the same sequences as the MCC339 strain (GenBank EU375804). Cases 2, 4, and 9 showed doublet bands of 191 and 138 bp in the VP1 PCR. Sequencing analysis revealed that these two bands corresponded to PCR products of primary and secondary amplification. None of the primer sets for nested PCR amplified DNA products in tissues extracted from JCV-positive progressive multifocal leukoencephalopathy (PML) or BKV-positive nephritis samples (Fig. 1). These data indicate the presence of MCPyV in six cases of Merkel cell carcinoma.

Quantitative Analysis of MCPyV in Merkel Cell Carcinoma

To determine the virus copy numbers in DNA samples, a real-time TaqMan PCR to detect the MCPyV gene was established. Based on the results of nested

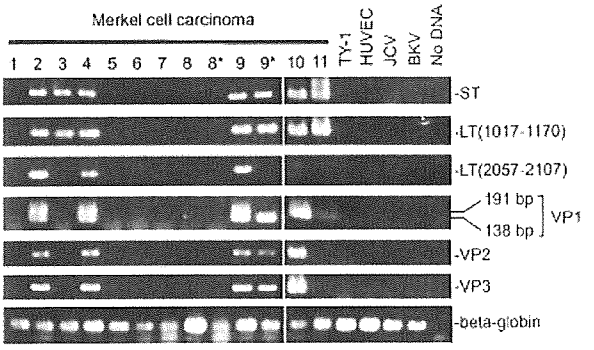

Fig. 1. Detection of MCPyV in Merkel cell carcinoma cases by nested PCR. Fragments of MCPyV were amplified with nested PCR in Merkel cell carcinoma cases. Thirteen samples of Merkel cell carcinoma were used. Sample nos. 8* and 9* are recurrent tumors of cases 8 and 9, respectively. TY-1, human herpesvirus-8-positive B cell line; HUVEC, human umbilical vascular endothelial cells; JCV, JCV-positive progressive multifocal leukoencephalopathy sample; BKV, BKV-positive nephritis sample. The two bands at 191 and 138 bp represent the PCR products of primary and secondary amplification, respectively. The lower panel shows single PCR for the β-globin gene.

PCR, the LT (1017–1170) region of MCPyV was selected as a target gene for real-time PCR. Amplification plots and standard curves revealed a linear relationship between copy numbers from 10 to 10^8 copies and cycle threshold (C_t), indicating that the dynamic range of the real-time PCRs was between 10 and 10^8 copies (data not shown). The MCPyV-LT genome assay uniformly detected 10 copies of pCR2.1-MCPyV-LT plasmid. PCR amplification of β-actin also uniformly detected 10 copies of the β-actin genome (data not shown). The specificity of the assay for MCPyV-LT was confirmed using a panel of DNAs from other polyomavirus (JCV, BKV, and SV40), human papillomavirus, herpes viruses (herpes simplex virus-1 and -2, varicella zoster virus, EBV, human cytomegalovirus, and HHV-6, -7, and -8), and cellular DNA from human cell lines (TY-1 and Raji, data not shown). Real-time PCR revealed that all six cases (seven samples) positive for MCPyV by nested PCR had 50–691 copies per 100 ng DNA (Table I). Compared with the results of cellular DNA (β-actin), the copy numbers in MCPyV-positive samples were estimated to in the range of 0.04–0.43 copies per cell (Table I).

Morphological Features of MCPyV-Positive Merkel Cell Carcinoma

Histological analysis of Merkel cell carcinoma cases revealed some morphological differences between MCPyV-positive and -negative Merkel cell carcinoma cases. All seven MCPyV-positive samples (cases 2, 3, 4, 9, 9*, 10, and 11) had common features such as round and vesicular nuclei with fine granular chromatin and small nucleoli. However, MCPyV-negative samples showed various morphologies. Some of the MCPyV-negative cases showed some similarities in morphology with MCPyV-positive samples; however, most of the MCPyV-negative samples had polygonal nuclei with light cytoplasm (Fig. 2). Chromatin was diffusely distributed in the nuclei, and the nucleoli were unclear in MCPyV-negative samples. MCPyV-positive cases also showed diffuse infiltration into the skin, whereas some of the MCPyV-negative cases showed duct differentiation. There were no significant differences in cytokeratin 20, NSE, or chromogranin expression between the MCPyV-positive and -negative Merkel cell carcinoma samples (Fig. 2 and data not shown). These morphological differences suggest differences in pathogenesis between MCPyV-positive and -negative Merkel cell carcinoma.

Prevalence of MCPyV in Various Diseases and Cell Lines

To clarify the prevalence of MCPyV, real-time PCR for MCPyV-LT was performed on DNAs extracted from various tissue samples (Table III). MCPyV was detected in three out of 49 (6.1%) cases of KS, but not in other diseases such as AIDS-related lymphoma, fulminant hepatitis, encephalitis, primary pulmonary hypertension, or necrotizing lymphadenitis. All 142 autopsy samples taken from various organs of 20 immunodeficient patients were negative for MCPyV with real-time PCR. In addition, all DNA samples extracted from 15 cell lines (seven B cell lines, TY-1, BCBL-1, Raji, Namalwa, Bjab, KS1, and OS1; three T cell lines, MT4, Molt4, and Jurkat; two monocyte cell lines, HL60, and THP1; one KS cell line, 22-KS; one endothelial cell line, HUVEC; one Marmoset cell line, B95-8) were negative for MCPyV (data not shown). These data indicate the low prevalence of MCPyV in Japan, and suggest that some cases of Merkel cell carcinoma and KS are associated with MCPyV infection.

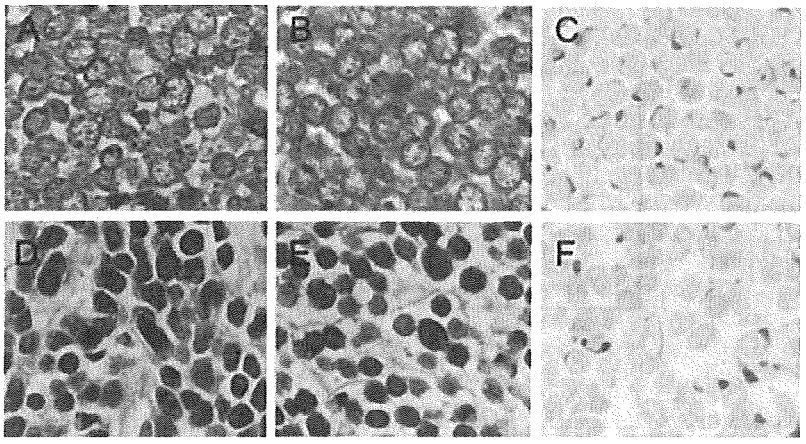

Fig. 2. Histology of MCPyV-positive and -negative Merkel cell carcinoma. **A–C**: MCPyV-positive Merkel cell carcinoma. HE staining of cases 2 (A) and 9 (B) shows round and vesicular nuclei with fine granular chromatin and small nucleoli. C: Cytokeratin 20 expression of case 2. **D–F**: MCPyV-negative Merkel cell carcinoma. HE staining of cases 5 (D) and 6 (E) shows dark and polymorphic nuclei with light cytoplasm. Chromatin in the polymorphic nuclei is diffuse, and the nucleoli are unclear. F: Cytokeratin 20 expression in case 6 is similar to the MCPyV-positive cases.

TABLE III. MCPyV Infection in Various Diseases

Sample	Positive/all	Percentage
Merkel cell carcinoma	6 (0)/11 (0)	54.5
KS	3 (1)/49 (16)	6.1
AIDS-related lymphoma	0 (0)/11 (11)	0
Fulminant hepatitis	0 (0)/9 (9)	0
Encephalitis	0 (0)/12 (12)	0
Including PML (JCV+)	0 (0)/4 (4)	0
BKV-positive nephritis	0 (0)/1 (1)	0
Primary effusion lymphoma	0 (0)/4 (4)	0
PPH	0 (0)/10 (0)	0
Necrotizing lymphadenitis	0 (0)/2 (2)	0
FDC sarcoma	0 (0)/1 (1)	0
AIDS autopsy		
Brain	0 (0)/15 (15)	0
Tongue	0 (0)/5 (5)	0
Submandibular gland	0 (0)/5 (5)	0
Lung	0 (0)/15 (15)	0
Lymph node	0 (0)/12 (12)	0
Heart	0 (0)/9 (9)	0
GI tract	0 (0)/13 (13)	0
Liver	0 (0)/16 (16)	0
Spleen	0 (0)/19 (19)	0
Pancreas	0 (0)/12 (12)	0
Kidney	0 (0)/14 (14)	0
Adrenal gland	0 (0)/7 (7)	0

KS, Kaposi's sarcoma; PML, progressive multifocal leukoencephalopathy; PPH, primary pulmonary hypertension; FDC, follicular dendritic cell; GI, gastrointestinal.
The number of frozen samples is shown in parentheses.

MCPyV Infection in KS Samples and Cloning of a Full-Length MCPyV Genome From a KS Case

Nested PCR was performed to confirm MCPyV infection in KS samples positive for MCPyV on real-time PCR. MCPyV fragments were detected in three KS cases using nested PCR (KS cases 3, 14, and 36 in Fig. 3A). However, nested PCR failed to detect VP1 and VP3 in KS cases 3 and 14, respectively. Sequencing analysis revealed that these products had sequences identical to those of Merkel cell carcinoma cases in the present study. The MCPyV-LT/β-actin copy numbers in these three KS samples were $1.3 \times 10^1/2.0 \times 10^4$, $3.3 \times 10^1/2.4 \times 10^5$, and $3.3 \times 10^1/1.8 \times 10^6$ per 100 ng DNA, respectively, suggesting low copy numbers (3.6×10^{-5}–1.2×10^{-3} copies per cell) compared with the Merkel cell carcinoma cases (Fig. 3B). Two (cases 14 and 36) of the MCPyV-positive cases with KS were AIDS-associated KS; however, the other case (case 3) was an HIV-negative patient. Because one MCPyV-positive KS case (case 36) was a frozen tissue sample, that sample was used to clone the full genome of MCPyV. PCR successfully amplified the full-length MCPyV genome with a primer set localized using the *Bam*HI site (1152 in GenBank EU375803) (primer set 1: MCV-*Bam*HI-1150F and MCV-*Bam*HI-1150R). PCR was also able to amplify almost the full-length of the MCPyV genome using a primer set localized to the origin region of MCPyV (primer set 2 MCV-F133 and MCV-R5325), and a 1,188-bp-fragment containing the origin region (primer set 3 MCV-VP3-F4932 and MCV-ST-R732), suggesting the presence of a MCPyV episome. The PCR product of full-length MCPyV genome was TA-cloned into pCR2.1 and two clones were sequenced. Sequence analysis revealed that the length of MCPyV genome was 5,418 bp. The two clones had the same sequence. This strain of MCPyV was designated as MCV-TKS (MCPyV-Tokyo Kaposi sarcoma) and registered in the GenBank (accession No. FJ464337). The sequence of MCV-TKS had 98% homology to MCC350 (GenBank EU375803). The motifs of LXXLL in CR1, HPDKGG in DnaJ, and LXCXE in the Rb binding site were conserved in the LT gene of MCV-TKS. The sequence of LT had a stop codon at 1,498, suggesting that MCV-TKS would produce a truncated form of LT [Shuda et al., 2008].

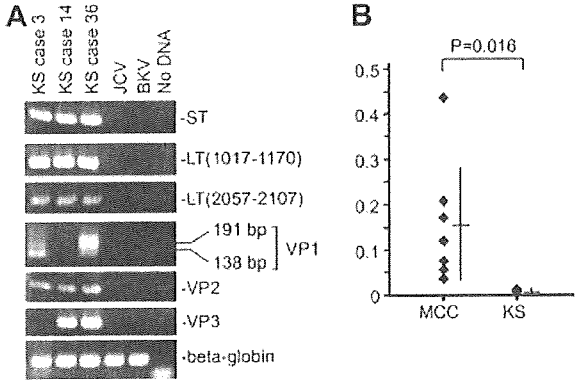

Fig. 3. Detection and cloning of MCPyV in KS cases. **A**: Fragments of MCPyV were amplified with nested PCR in three KS cases. JCV, JCV-positive PML sample; BKV, BKV-positive nephritis sample. **B**: Comparison of MCPyV copy numbers between Merkel cell carcinoma (MCC) and Kaposi's sarcoma (KS) samples with real-time PCR. The *y*-axis shows copy numbers per cell. The horizontal and vertical lines indicate means and standard deviation, respectively. The *P*-value was calculated with the Mann–Whitney test.

DISCUSSION

In the present study, the presence of MCPyV was demonstrated in Japanese cases of Merkel cell carcinoma. This indicates that MCPyV is distributed not only in the US, Europe, and Australia, but also worldwide. The rate of MCPyV in Japanese Merkel cell carcinoma cases (55%) was lower than that of the United States and European cases (69–100%), but higher than in Australia (24%) [Feng et al., 2008; Foulongne et al., 2008; Kassem et al., 2008; Becker et al., 2009; Duncavage et al., 2009; Garneski et al., 2009; Sastre-Garau et al., 2009]. In addition to that of Merkel cell carcinoma, the rate of MCPyV in KS (6%) was also lower than in the United States (16%) [Feng et al., 2008]. A US group detected MCPyV in some control tissues obtained from the gastrointestinal tract with PCR-Southern blot hybridization [Feng et al., 2008]. However, in the present study, all of the samples, except for Merkel cell carcinoma and KS samples, were negative for MCPyV. Taken together, these data suggest a lower infection rate of MCPyV in the Japanese population than in the US. Because Merkel cell carcinoma occurs more

frequently in Caucasians than in other races [Agelli and Clegg, 2003], it is possible that the distribution of MCPyV varies among races.

Nested PCR failed to detect VP1–3 and LT (2057–2107) in some MCPyV-positive cases of Merkel cell carcinoma including a recurrent case of MCPyV-positive tumor (Fig. 1). VP1 or VP3 was not detected in two MCPyV-positive cases of KS (Fig. 3A). There are some possible interpretations of these results. Recent reports demonstrated mutations in the LT gene and a unique deletion in the VP1 gene [Kassem et al., 2008; Shuda et al., 2008]. Thus, some mutations or deletions might exist in the primer regions of VP1–3 and LT of MCPyV, as in other polyomavirus such as JCV, BKV, and human papillomavirus (HPV).

Morphological differences between MCPyV-positive and -negative cases were found in the present study. MCPyV-positive cases can be categorized into one group with a typical morphology, whereas the MCPyV-negative cases had a mixed morphology. These morphological differences imply direct tumorigenesis by MCPyV infection in the MCPyV-positive cases and more complicated mechanisms in the MCPyV-negative cases. No rosette formation or ductal differentiation was observed in the MCPyV-positive cases, suggesting that MCPyV infection might be associated with differentiation of Merkel cells. A recent gene expression analysis using microarrays revealed that Merkel cell carcinoma might comprise two subtypes, namely the classic and variant types [Van Gele et al., 2004]. Although it is presumed that MCPyV infection may be associated with such subtypes, more cases of Merkel cell carcinoma are required to clarify the morphological features and presence of MCPyV infection. In addition, a recent immunohistochemical study demonstrated the expression of MCPyV-LT protein in tumor cells in Merkel cell carcinoma with a high number of MCPyV copies per cell, suggesting that MCPyV causes a subset of Merkel cell carcinoma [Shuda et al., 2009]. The morphological differences between MCPyV-positive and -negative cases support the presence of a MCPyV-negative subset of Merkel cell carcinoma.

The data for virus copy number provide valuable insights into the pathogenesis of Merkel cell carcinoma. In the present study, nested PCR and real-time PCR, but not PCR-Southern blot hybridization, was performed to detect MCPyV in clinical samples. Because DNA is always cleaved into small fragments in formalin-fixed tissues, it is difficult to amplify long DNA fragments. Our nested PCR and real-time PCR targeted fragments of MCPyV of <250 bp. The results of nested PCR for the LT gene and real-time PCR on clinical samples were well-correlated with each other in the present study. Because other studies have demonstrated that MCPyV-DNA is integrated into genomic DNA, at least one or two copies of MCPyV per cells are expected [Feng et al., 2008; Sastre-Garau et al., 2009]. On the other hand, it was demonstrated that Merkel cell carcinoma cases with a low copy number of MCPyV did not express the LT antigen [Shuda et al., 2009]. Because Merkel cell carcinoma tissue samples contained various proportions of tumor cells and normal cells, it is difficult to determine the accurate virus copy number per cell [Asahi-Ozaki et al., 2006]. The Merkel cell carcinoma tissue samples in the present study were rich in tumor cells and contained relatively few normal cells. Thus, the copy numbers of MCPyV in Merkel cell carcinoma (0.04–0.43 per cell) in the present study suggest the presence of Merkel cell carcinoma in cases with a low copy number of MCPyV. It was not possible to examine the clonal integration of MCPyV in DNA samples extracted from formalin-fixed and paraffin-embedded tissues. Future studies on frozen tissue samples will reveal the association between pathogenesis and MCPyV integration.

Here, MCPyV was detected in three cases of KS and cloning a full-length MCPyV genome. A previous report also demonstrated the presence of MCPyV in some KS cases without HIV infection [Feng et al., 2008]. Therefore, there might be some association between MCPyV infection and KS pathogenesis. There was no common feature between the three MCPyV-positive KS cases, including HIV-status. Human herpesvirus-8 was identified in all KS cases examined (data not shown). However, none of the Merkel cell carcinoma cases used in the present study were positive for human herpesvirus-8, as determined by PCR (data not shown). The results using AIDS autopsy samples also suggest that HIV status was not correlated with MCPyV infection. The low MCPyV copy number and the presence of episomal MCPyV in the KS samples suggest an indirect association between MCPyV and KS pathogenesis. MCV-TKS identified in the present study is the first isolate of MCPyV derived from a KS sample. The sequence data for MCV-TKS suggested that the LT gene would produce truncated LT, which is associated with the pathogenesis of Merkel cell carcinoma [Shuda et al., 2008]. However, to determine whether MCPyV infection is a risk factor for KS, the MCPyV status in Merkel cell in KS patients should be investigated.

In conclusion, MCPyV was detected in Japanese cases with Merkel cell carcinoma and KS. Although MCPyV infection appears to be rare in the Japanese population, this study provides evidence that MCPyV is spread worldwide, and that MCPyV is associated with pathogenesis in some Merkel cell carcinoma cases.

ACKNOWLEDGMENTS

We thank Dr. Akira Suzuki and Dr. Yuichiro Fukasawa, Department of Clinical Laboratory, KKR Sapporo Medical Center, Toshihiko Iizuka and Hisako Endo, Department of Pathology, International Medical Center of Japan, for providing clinical samples.

REFERENCES

Agelli M, Clegg LX. 2003. Epidemiology of primary Merkel cell carcinoma in the United States. J Am Acad Dermatol 49:832–841.

Asahi-Ozaki Y, Sato Y, Kanno T, Sata T, Katano H. 2006. Quantitative analysis of Kaposi sarcoma-associated herpesvirus (KSHV) in KSHV-associated diseases. J Infect Dis 193:773–782.

Becker JC, Houben R, Ugurel S, Trefzer U, Pfohler C, Schrama D. 2009. MC polyomavirus is frequently present in Merkel cell carcinoma of European patients. J Invest Dermatol 129:248–250.

Bialasiewicz S, Lambert SB, Whiley DM, Nissen MD, Sloots TP. 2009. Merkel cell polyomavirus DNA in respiratory specimens from children and adults. Emerg Infect Dis 15:492–494.

Bluemn EG, Paulson KG, Higgins EE, Sun Y, Nghiem P, Nelson PS. 2009. Merkel cell polyomavirus is not detected in prostate cancers, surrounding stroma, or benign prostate controls. J Clin Virol 44: 164–166.

Duncavage EJ, Zehnbauer BA, Pfeifer JD. 2009. Prevalence of Merkel cell polyomavirus in Merkel cell carcinoma. Mod Pathol 22:516–521.

Feng H, Shuda M, Chang Y, Moore PS. 2008. Clonal integration of a polyomavirus in human Merkel cell carcinoma. Science 319:1096–1100.

Fernandez-Figueras MT, Puig L, Musulen E, Gilaberte M, Lerma E, Serrano S, Ferrandiz C, Ariza A. 2007. Expression profiles associated with aggressive behavior in Merkel cell carcinoma. Mod Pathol 20:90–101.

Foulongne V, Kluger N, Dereure O, Brieu N, Guillot B, Segondy M. 2008. Merkel cell polyomavirus and Merkel cell carcinoma, France. Emerg Infect Dis 14:1491–1493.

Garneski KM, Warcola AH, Feng Q, Kiviat NB, Leonard JH, Nghiem P. 2009. Merkel cell polyomavirus is more frequently present in North American than Australian Merkel cell carcinoma tumors. J Invest Dermatol 129:246–248.

Giraud G, Ramqvist T, Ragnarsson-Olding B, Dalianis T. 2008. DNA from BK virus and JC virus and from KI, WU, and MC polyomaviruses as well as from simian virus 40 is not detected in non-UV-light-associated primary malignant melanomas of mucous membranes. J Clin Microbiol 46:3595–3598.

Goh S, Lindau C, Tiveljung-Lindell A, Allander T. 2009. Merkel cell polyomavirus in respiratory tract secretions. Emerg Infect Dis 15: 489–491.

Kassem A, Schopflin A, Diaz C, Weyers W, Stickeler E, Werner M, Zur Hausen A. 2008. Frequent detection of Merkel cell polyomavirus in human Merkel cell carcinomas and identification of a unique deletion in the VP1 gene. Cancer Res 68:5009–5013.

Katano H, Sato Y, Sata T. 2001. Expression of p53 and human herpesvirus 8 (HHV-8)-encoded latency-associated nuclear antigen (LANA) with inhibition of apoptosis in HHV-8-associated malignancies. Cancer 92:3076–3084.

Kuramochi H, Hayashi K, Uchida K, Miyakura S, Shimizu D, Vallbohmer D, Park S, Danenberg KD, Takasaki K, Danenberg PV. 2006. Vascular endothelial growth factor messenger RNA expression level is preserved in liver metastases compared with corresponding primary colorectal cancer. Clin Cancer Res 12:29–33.

Lemos B, Nghiem P. 2007. Merkel cell carcinoma: More deaths but still no pathway to blame. J Invest Dermatol 127:2100–2103.

Pectasides D, Pectasides M, Economopoulos T. 2006. Merkel cell cancer of the skin. Ann Oncol 17:1489–1495.

Ridd K, Yu S, Bastian BC. 2009. The presence of polyomavirus in non-melanoma skin cancer in organ transplant recipients is rare. J Invest Dermatol 129:250–252.

Sastre-Garau X, Peter M, Avril MF, Laude H, Couturier J, Rozenberg F, Almeida A, Boitier F, Carlotti A, Couturaud B, Dupin N. 2009. Merkel cell carcinoma of the skin: Pathological and molecular evidence for a causative role of MCV in oncogenesis. J Pathol 218: 48–56.

Sharp CP, Norja P, Anthony I, Bell JE, Simmonds P. 2009. Reactivation and mutation of newly discovered WU, KI, and Merkel cell carcinoma polyomaviruses in immunosuppressed individuals. J Infect Dis 199:398–404.

Shuda M, Feng H, Kwun HJ, Rosen ST, Gjoerup O, Moore PS, Chang Y. 2008. T antigen mutations are a human tumor-specific signature for Merkel cell polyomavirus. Proc Natl Acad Sci USA 105:16272–16277.

Shuda M, Arora R, Kwun HJ, Feng H, Sarid R, Fernandez-Figueras MT, Tolstov Y, Gjoerup O, Mansukhani MM, Swerdlow SH, Chaudhary PM, Kirkwood JM, Nalesnik MA, Kant JA, Weiss LM, Moore PS, Chang Y. 2009. Human Merkel cell polyomavirus infection I. MCV T antigen expression in Merkel cell carcinoma, lymphoid tissues and lymphoid tumors. Int J Cancer 125:1243–1249.

Skelton HG, Smith KJ, Hitchcock CL, McCarthy WF, Lupton GP, Graham JH. 1997. Merkel cell carcinoma: Analysis of clinical, histologic, and immunohistologic features of 132 cases with relation to survival. J Am Acad Dermatol 37:734–739.

Van Gele M, Boyle GM, Cook AL, Vandesompele J, Boonefaes T, Rottiers P, Van Roy N, De Paepe A, Parsons PG, Leonard JH, Speleman F. 2004. Gene-expression profiling reveals distinct expression patterns for Classic versus Variant Merkel cell phenotypes and new classifier genes to distinguish Merkel cell from small-cell lung carcinoma. Oncogene 23:2732–2742.

zur Hausen H. 2008. A specific signature of Merkel cell polyomavirus persistence in human cancer cells. Proc Natl Acad Sci USA 105: 16063–16064.

Int. J. Cancer: **125,** 1464–1472 (2009)

Biscoclaurine alkaloid cepharanthine inhibits the growth of primary effusion lymphoma *in vitro* and *in vivo* and induces apoptosis *via* suppression of the NF-κB pathway

Naoko Takahashi-Makise[1], Shinya Suzu[1], Masateru Hiyoshi[1], Takeo Ohsugi[2], Harutaka Katano[3], Kazuo Umezawa[4] and Seiji Okada[1]*

[1]*Division of Hematopoiesis, Center for AIDS Research, Kumamoto University, Honjo, Kumamoto, Japan*
[2]*Division of Microbiology and Genetics, Center for Animal Resources and Development, Institute of Resource Development and Analysis, Kumamoto University, Honjo, Kumamoto, Japan*
[3]*Department of Pathology, National Institute of Infectious Diseases, Toyama, Shinjuku, Tokyo, Japan*
[4]*Department of Applied Chemistry, Faculty of Science and Technology, Keio University, Hiyoshi, Kohoku-Ku, Yokohama, Japan*

Primary effusion lymphoma (PEL) is a unique and recently identified non-Hodgkin's lymphoma that was originally identified in patients with AIDS. PEL is caused by the Kaposi sarcoma-associated herpes virus (KSHV/HHV-8) and shows a peculiar presentation involving liquid growth in the serous body cavity and a poor prognosis. As the nuclear factor (NF)-κB pathway is activated in PEL and plays a central role in oncogenesis, we examined the effect of a biscoclaurine alkaloid, cepharanthine (CEP) on PEL derived cell lines (BCBL-1, TY-1 and RM-P1), *in vitro* and *in vivo*. An methylthiotetrazole assay revealed that the cell proliferation of PEL cell lines was significantly suppressed by the addition of CEP (1–10 μg/ml). CEP also inhibited NF-κB activation and induced apoptotic cell death in PEL cell lines. We established a PEL animal model by intraperitoneal injection of BCBL-1, which led to the development of ascites and diffuse infiltration of organs, without obvious solid lymphoma formation, which resembles the diffuse nature of human PEL. Intraperitoneal administration of CEP inhibited ascites formation and diffuse infiltration of BCBL-1 without significant systemic toxicity in this model. These results indicate that NF-κB could be an ideal molecular target for treating PEL and that CEP is quite useful as a unique therapeutic agent for PEL.

Key words: NF-κB; primary effusion lymphoma; cepharanthine; animal model

Primary effusion lymphoma (PEL) is a subtype of non-Hodgkin's B cell lymphoma that mainly presents in patients with advanced AIDS, but is sometimes also found in immunosuppressed patients such as those who have undergo organ transplantation.[1,2] Among AIDS-related NHLs, PEL generally has an extremely aggressive clinical course with a median survival of only 3 months.[3] PEL usually presents as a lymphomatous effusion in body cavities and is caused by Kaposi sarcoma-associated herpes virus (KSVH/HHV-8).[1] A number of constitutively activated signaling pathways play critical roles in the survival and growth of PEL cells. These include nuclear factor (NF)-κB, JAK/STAT and PI3 kinase.[4–6] KSHV/HHV-8 encodes a virus Fas-associated death domain-like interleukin-1β-converting enzyme (FLICE) inhibitory protein (vFLIP) that has the ability to activate the NF-κB pathway.[7–9] vFLIP has been shown to bind to the IKK complex to induce constitutive kinase activation,[10] and as a result, PEL cells have high levels of nuclear NF-κB activity, whereas inhibition of NF-κB induces apoptosis in PEL cells.[5,11] These studies support the idea that vFLIP-mediated NF-κB activation is necessary for the survival of PEL cells and that this pathway represents a target for molecular therapy for this disease.

Cepharanthine (CEP) is a biscoclaurine (bisbenzylisoquinoline) amphipathic alkaloid that was isolated from *Stephania cepharantha* Hayata. CEP and extracts from this plant are widely used, primarily in Japan, to treat a variety of acute and chronic diseases without any serious side effects.[12] CEP is known to possess various biological and pharmacological activities, including membrane-stabilizing,[13,14] immunomodulatory,[15] and anti-inflammatory activities.[16] CEP also has antiproliferative and proapoptotic effects against a diverse range of tumors both *in vitro* and *in vivo*.[17–21] In addition, this agent has been shown to inhibit the activation of NF-κB,[22,23] a transcription factor of critical importance in the regulation of cell growth and survival.

In the present study, we investigated the antitumor activity of CEP against human PEL cell lines. CEP inhibits constitutive active NF-κB, leading to apoptosis in PEL. Our findings provide the experimental basis for utilizing CEP against tumors activated by NF-κB.

Material and methods

Cell lines and reagents

The human PEL cell lines, BCBL-1 (obtained through the AIDS Research and Reference Reagent Program, Division of AIDS, NIAID, NIH),[24] TY-1[25] and RM-P1 (a kind gift of Dr. T. Taira, University of the Ryukyus, Japan),[26] and non-PEL human B cell lines, BALL-1 (a kind gift of Dr. K. Kuwahara, Kumamoto University, Japan), RAMOS (a kind gift of Dr. K. Kuwahara, Kumamoto University, Japan) and Raji (obtained from RIKEN Cell Bank, Tsukuba, Japan) were maintained in RPMI1640 supplemented with 10% heat inactivated fetal calf serum, penicillin (100 U/ml) and streptomycin (100 μg/ml) in a humidified incubator at 37°C and 5% CO_2. CEP was kindly provided by Kaken Shoyaku Co., Ltd. (Tokyo, Japan). DHMEQ is a NF-κB inhibitor that acts at the level of nuclear translocation of NF-κB.[27]

Tetrazolium dye methylthiotetrazole assay

The antiproliferative effects of CEP against PEL and non-PEL B cell lines were measured by the methylthiotetrazole (MTT) method (Sigma, St. Louis, MO). Briefly, 2×10^4 cells were incubated in triplicate in a 96-well microculture plate in the presence of different concentrations of CEP in a final volume of 0.1 ml for 48 hr at 37°C. Subsequently, MTT (0.5 mg/ml final concentration) was added to each well. After 3 hr of additional incubation, 100 μl of a solution containing 10% SDS plus 0.01 N HCl were added to dissolve the crystal. The absorption values at 570 nm were determined with an automatic enzyme-linked immnosorbent assay (ELISA) plate reader (Multiskan, Thermo ElectronVantaa, Finland). Values are normalized to the untreated (control) samples.

Grant sponsor: Ministry of Health, Labour and Welfare of Japan; Grant number: H19-AIDS-003; Grant sponsor: Ministry of Education, Science, Sports, and Culture of Japan.
***Correspondence to:** Division of Hematopoiesis, Center for AIDS Research, Kumamoto University, 2-2-1 Honjo, Kumamoto, 860-0811, Japan. Fax: +81-96-373-6523. E-mail: okadas@kumamoto-u.ac.jp
Received 20 September 2008; Revised 31 March 2009; Accepted after revision 7 April 2009
DOI 10.1002/ijc.24521
Published online 23 April 2009 in Wiley InterScience (www.interscience.wiley.com).

Cell cycle analysis

For cell cycle analysis, after PEL cells were treated with CEP for18 hr, the cells were incubated in hypotonic lysing buffer [0.1% sodium citrate, 0.1% Triton X, 0.1% RNase A and 50 μg/ml propidium iodide (PI)] at 4°C for 4 hr.[28] DNA content in each cell was analyzed on LSR II flow cytometer (BD Bioscience, San Jose, CA). Data were analyzed on FlowJo software (Tree Star, San Carlos, CA).

Annexin V assay

Apoptosis was quantified using the Annexin V: PE apoptosis detection kit I (BD Biosciences). Briefly, after treatment with CEP, cells were harvested, washed and then incubated with Annexin V-PE and 7-AAD for 15 min in the dark, before being analyzed on a LSR II cytometer.

Caspase activity measurements with flowcytometry

The active caspase 3 activity was measured using PhiPhiLux-G2D2 (OncoImmunin, Gaithersburg, MD)[29] according to the manufacturer's instructions. Briefly, CEP treated or untreated cells were incubated with 10 μM caspase substrate for 60 min, added 2 μl/ml of PI and analyzed by LSR II. Data were analyzed on FlowJo software, expressed casepase 3 positive cellular events among PI-negative (living) cells.

Western blot analysis

BCBL-1, TY-1 and RM-P1 cells with or without treatment of 10 μg/ml of CEP for 24 hr were collected and washed in cold PBS before the addition of 400 μl of cold buffer A (10 mM HEPES-KOH pH 7.9, 1.5 mM $MgCl_2$, 10 mM KCl, 0.1% NP-40, 0.5 mM DTT, 0.5 mM PMSF, 2 μg/ml pepstatin A, 2 μg/ml aprotinin and 2 μg/ml leupeptin). After incubation on ice for 10 min, the samples were vortexed for 10 sec. Nuclei were pelleted by centrifugation at 5,000 rpm for 1 min and washed once with buffer A. Fifty microliters of buffer C (50 mM HEPES-KOH pH 7.9, 10% glycerol, 420 mM KCl, 5 mM $MgCl_2$, 0.1 mM EDTA, 1 mM DTT, 0.5 mM PMSF, 2 μg/ml pepstatin A, 2 μg/ml aprotinin and 2 μg/ml leupeptin) were added to the nuclei and incubated on ice for 30 min. Nuclear extracts were obtained by centrifugation at 15,000 rpm for 15 min, then the nuclear extracts (40 μg protein) were separated by 10% SDS-PAGE and blotted onto a PVDF membrane (GE Healthcare, Tokyo, Japan). Detection was performed using Enhanced Chemiluminescence Western Blotting Detection System (ECL, GE Healthcare Bio-Science, Buckinghamshire, UK). Primary antibodies used were as follows: anti-p65 (F-6), anti-phospho(Ser311)-p65, anti-IκBα(C-21), anti-phospho(Ser32)-IκBα (B-6), anti-IKKαβ (H-479), anti-phospho(Thr23)-IKKαβ, anti-Actin(C-2) and anti-Histone H1(N-16) (Santa CruZ Biotechnology, Santa Cruz, CA).

Quantification of the Western blots was performed using NIH Image software (NIH, Bethesda, MD). Relative density was evaluated and normalized with actin or Histone H1.

Measurement of nuclear active NF-κB p65

PEL cells are treated with CEP for 18 hr and nuclear active NF-κB p65 was measured using an ELISA according to the manufactures's protocol (IMGENEX, San Diego, CA). In brief, the cells were centrifuged at 400*g* for 1 min and washed with cold phosphate buffered saline (PBS). The cells were lyzed by 400 μl of hypotonic buffer and 30 μl of 10% NP-40 was added. The mixture was centrifuged at 18,000*g* for 30 sec. The pellet was resuspended in 220 μl of nuclear extraction buffer and centrifuged at 18,000*g* for 1 min. The supernatant was used as nuclear extract. The anti-p65 antibody coated plate captured nuclear or cytoplasmic free p65 of samples (0.5–1 mg/ml of protein) and the amount of bound p65 was detected by adding a secondary antibody followed by alkaline phosphatase-conjugated secondary antibody. The absorbance value for each well was determined at 405 nm by a microplate reader (Bio-Rad). The relative activity of NF-κB is expressed as a percentage measured in control cells that were not treated with CEP.[30,31]

Electrophoretic mobility shift assay

The nuclear extracts from BCBL-1 cells were prepared using NF-κB/p65 ActiveELISA (IMGENEX). BCBL-1 cells that had been treated with CEP for the indicated period were collected and washed with PBS before 1× hypotonic buffer (1 ml) was added and then they were incubated on ice for 15 min. Fifty microliters of 10% detergent solution were added to the samples, and nuclei were collected by centrifugation at 14,000 rpm for 30 sec. One hundred microliters of nuclear lysis buffer were added to the nuclei, which were then incubated on ice for 30 min. Nuclear extracts were obtained by centrifugation at 14,000 rpm for 10 min. An electrophoretic mobility shift assay (EMSA) was performed using a 2nd generation DIG Gel Shit Kit (Roche Diagnostics, Mannheim, Germany). Briefly, double-stranded oligonucleotide probes containing the mouse immunoglobulin kappa (Igκ) light-chain NF-κB consensus site were purchased from Promega (Madison, WI). The oligonucleotide was 3′ end-labeled with a digoxigenin-11-ddUTP. The nuclear extract (10 μg protein) from BCBL-1 cells was incubated with 1 μg of poly[d(I-C)], 0.1 μg of poly-L-lysine and DIG-labeled oligonucleotide in binding buffer [20 mM HEPES pH 7.6, 1 mM EDTA, 10 mM $(NH_4)_2SO_4$, 0.2% Tween 20 and 30 mM KCl] for 15 min at 25°C. After the incubation, 5× loading buffer (0.25× TBE and 60% glycerol) was added, and the samples were separated on 5% acrylamide gel in 0.5× TBE buffer. The oligonucleotide was electroblotted onto a positively charged nylon membrane (Roche Diagnostics, Mannheim, Germany) and immunodetected using anti-digoxigenin-AP.

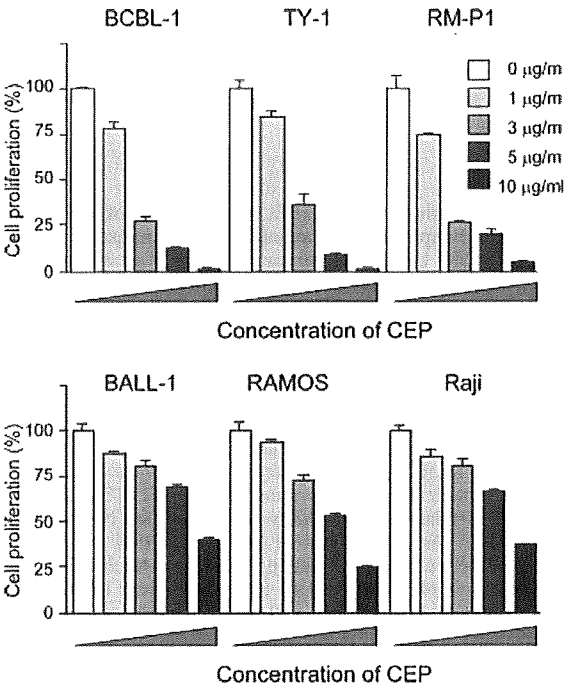

FIGURE 1 – CEP inhibits the proliferation of PEL cells. The PEL cell lines (BCBL-1, TY-1 and RM-P1) and non-PEL B cell lines (BALL-1, RAMOS and Raji) were incubated with 1, 3, 5, 10 μg/ml CEP for 48 hr. A cell proliferation assay was carried out using MTT as described in Material and methods section. One representative result from 3 independent experiments is shown.

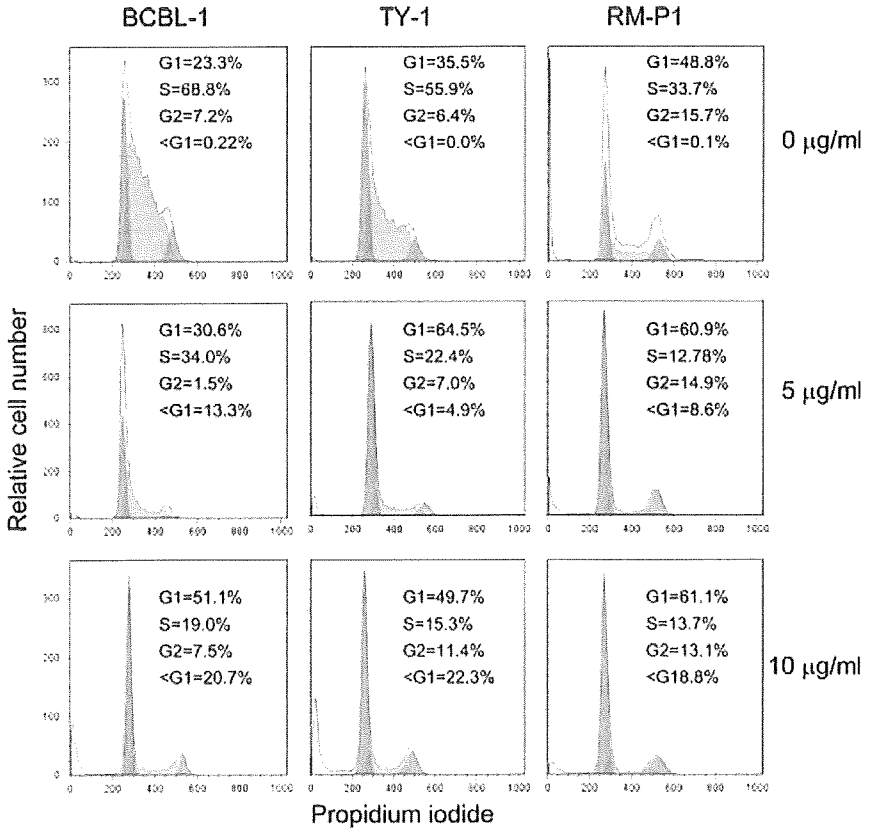

FIGURE 2 – CEP causes cell cycle arrest of PEL cells. The PEL cell lines BCBL-1, TY-1 and RM-P1 were treated with CEP (5 or 10 μg/ml) for 18 hr, and DNA histograms were determined and the cell cycle was analyzed using FlowJo software. One representative result from 3 independent experiments is shown. [Color figure can be viewed in the online issue, which is available at www.interscience.wiley.com.]

Xenograft mouse model

NOD/Scid/Jak3 deficient (NOJ) mice were established by backcrossing Jak3deficeint mice[32] with the NOD.Cg.-Prkdc^{scid} strain for 10 generations.[33] NOJ male mice 8-to 10-week-old were housed and monitored in our animal research facility according to the institutional guidelines. All experimental procedures and protocols were approved by the Institutional Animal Care and Use Committee at Kumamoto University. NOJ mice were intraperitoneally inoculated with 7×10^6 BCBL-1 cells suspended in 200 μl PBS. Then the mice were treated with intraperitoneal injections of PBS or CEP (10 mg/kg per day). Tumor burdens were evaluated by measuring the body weight and ascites.

Immunohistochemistry

To investigate the expression of KSHV/HHV-8 ORF73 (LANA) protein, tissue samples were fixed with 10% neutral-buffered formalin, embedded in paraffin and cut into 4-μm sections. The sections were deparaffinized by sequential immersion in xylene and ethanol and rehydrated in distilled water. They were then irradiated for 15 min in a microwave oven for antigen retrieval. Endogenous peroxidase activity was blocked by immersing the sections in methanol/0.6% H_2O_2 for 30 min at room temperature. Affinity-purified PA1-73N antibody,[34] diluted 1:3,000 in PBS/5% bovine serum albumin (BSA), was then applied, and the sections were incubated overnight at 4°C. After washing in PBS twice, the second and third reactions and the amplification procedure were performed using kits according to the manufacturer's instructions (catalyzed signal amplification system kit; DAKO, Copenhagen, Denmark). The signal was visualized using 0.2 mg/ml diaminobenzidine and 0.015% H_2O_2 in 0.05 mol/l Tris-HCl, pH 7.6.

Measurement of HHV-8 genome by real-time PCR

DNA was extracted from the lung, liver and spleen of CEP-treated and untreated mice. Copy number of KSHV ORF26 was measured with a Taqman real-time PCR.[35] The real-time PCR assay used forward (5′-CTCGAATCCAACGGATTTGAC-3′) and reverse (5′-TGCTGCAGAATAGCGTGCC-3′) primers (Oligos Etc., Wilsonville, OR) and the fluorogenic Taqman probe (5′-CCATGGTCGTGCCGCAGCA-3′; PE Applied Biosystems, Foster City, CA) to amplify and detect a 74-base pair amplicon in the KSHV minor capsid protein gene (open reading frame 26, from nucleotides 47,311 to 47,384 of the KSHV genome).

Treatment of Balb/c mice with CEP

Eight-week-old female Balb/c mice were obtained from Clea Japan (Tokyo, Japan). Mice were treated with intraperitoneal injections of PBS or CEP (10 mg/kg per day) for 21 consecutive days. Splenocytes were harvested, counted the cell numbers and stained with anti-mouse CD3-FITC and anti-mouse CD19-PE (eBiosciences, San Diego, CA).The cells were analyzed on LSR II flow cytometer, and data were analyzed on FlowJo software.

Statistical analysis

All assays were performed in triplicates and expressed as mean values ± SE. The statistical significance of the differences observed between experimental groups was determined using the Student *t* test. *p* values less than 0.05 were considered significant.

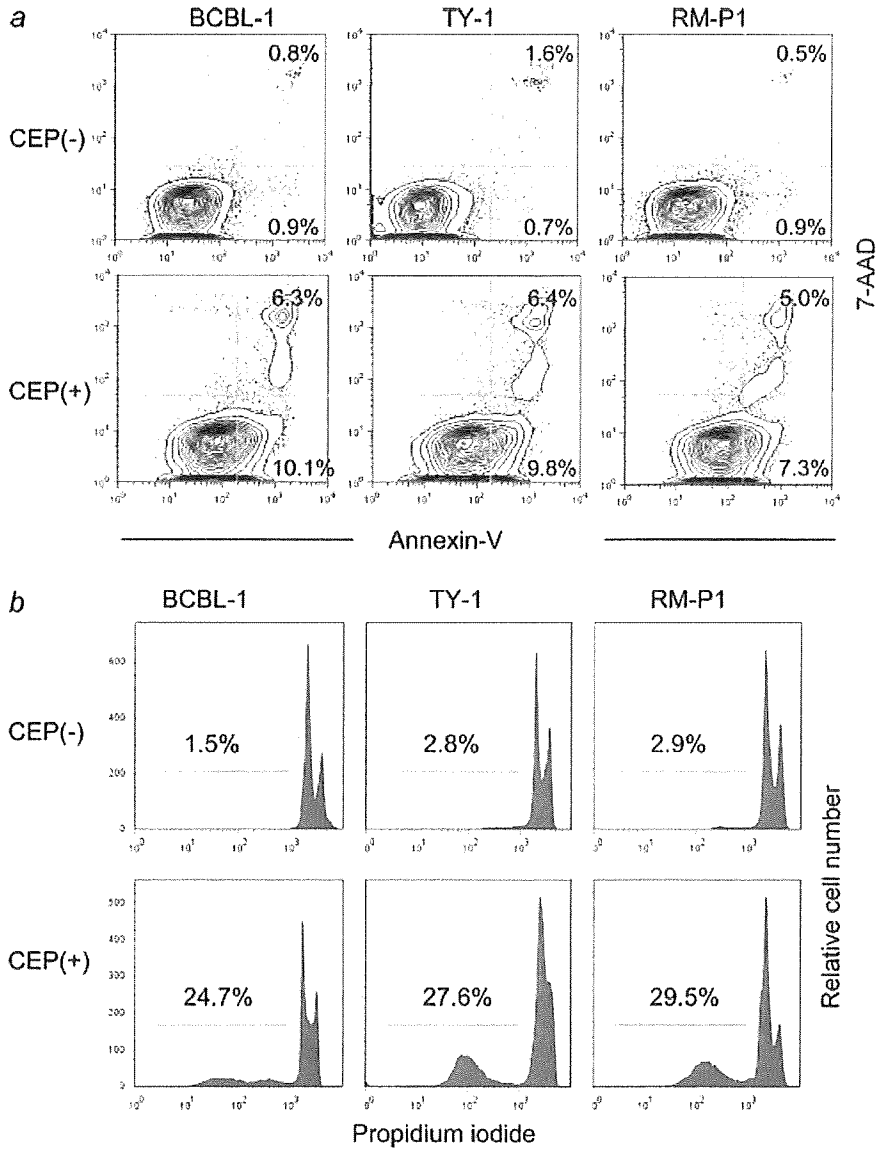

FIGURE 3 – CEP causes apoptosis of PEL cells. (*a*) CEP-induced apopotosis as detected by Annexin V and 7-AAD dual staining. The PEL cell lines BCBL-1, TY-1 and RM-P1 were treated with CEP (10 μg/ml) for 24 hr and were subsequently stained with Annexin-PE and 7-AAD before being analyzed by flow cytometry. (*b*) Apoptosis was determined by flow cytometric analysis of DNA fragmentation of PI stained nuclei. One representative result from 3 independent experiments is shown.

Results

CEP causes a dose-dependent inhibition of proliferation and apoptosis of PEL cell lines

We initially sought to determine whether CEP treatment leads to the inhibition of PEL cell proliferation. Three PEL cell lines (BCBL-1, TY-1 and RM-P1) and 3 non-PEL B cell lines (Ball-1, RAMOS and Raji) were cultured in the presence of 1, 3, 5 and 10 μg/ml CEP for 48 hr, and proliferation was analyzed by MTT assays. Figure 1 shows that as the dose of CEP increased from 1 to 10 μg/ml, cell growth inhibition increased in a dose-dependent fashion in all PEL cell lines and non-PEL B cell lines. PEL cell lines were more sensitive than non-PEL B cell lines against CEP treatment. In subsequent experiments, we determined whether the observed suppressive effects of CEP in MTT assay were due to induction of cell cycle arrest or apoptosis. As shown in Figure 2, CEP treatment for 18 hr induced cell cycle arrest with dose-dependent manner. We used Annexin V and 7-AAD dual staining to detect apoptosis. Annexin positive 7-AAD negative fraction represents the early phase of apoptosis whereas Annexin positive 7-AAD positive fraction represents the late phase of apoptosis and necrosis.[36] As shown in Figure 3*a*, 10 μg/ml CEP treatment for 24 hr caused apoptosis in all cell line tested. The sub-G1 population of cells (apoptotic cells)[28,37] increased with CEP treatment (Fig. 3*b*), indicating the PEL cells fell into apoptosis. Next, we measured the activation of caspase 3 to further confirm that CEP induced apoptosis in PEL cells. As shown in Figure 4, CEP treatment of PEL cells induced activation of caspase 3, a hallmark of cells undergoing apoptosis.[29]

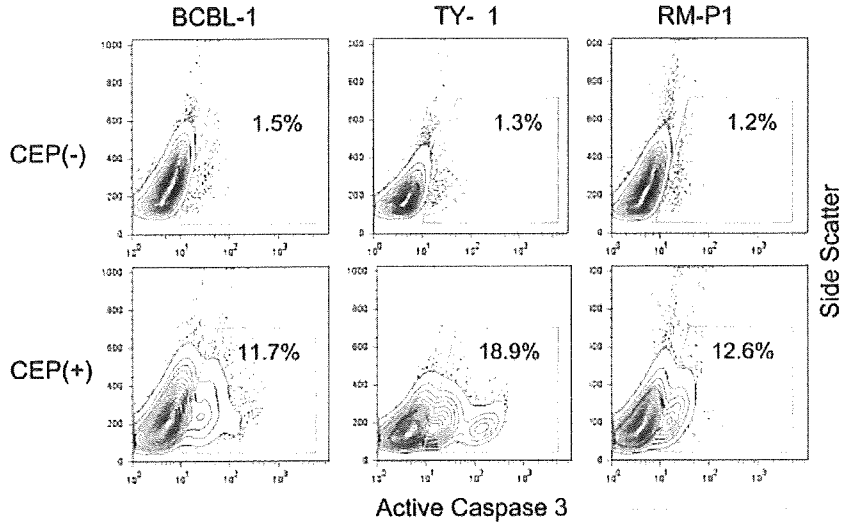

FIGURE 4 – CEP induces apoptosis of PEL cell *via* Caspase-3 dependent pathway. The PEL cells BCBL-1, TY-1 and RM-P1 were treated with CEP (10 μg/ml) for 24 hr and were subsequently stained with caspase-3 before being analyzed by flow cytometry. One representative result from 3 independent experiments is shown.

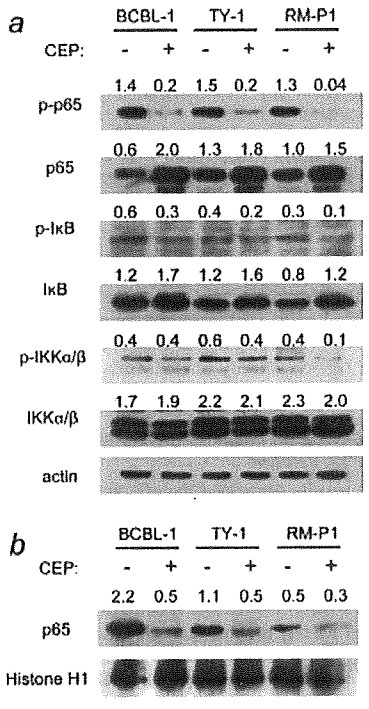

FIGURE 5 – Inhibitory effects of CEP on the expression of NF-κB pathways. (*a*) The PEL cell lines BCBL-1, TY-1 and RM-P1 were treated with CEP (10 μg/ml) for 24 hr and total proteins were extracted and Western blot was performed. The numbers indicate the relative expression of each protein level normalized with actin. (*b*) The PEL cell lines BCBL-1, TY-1 and RM-P1 were treated with CEP (10 μg/ml) for 24 hr and nuclear proteins were extracted and Western blot was performed to detect the NF-κB p65. The numbers indicate the relative expression of p65 normalized with Histone H1. One representative result from 3 independent experiments is shown.

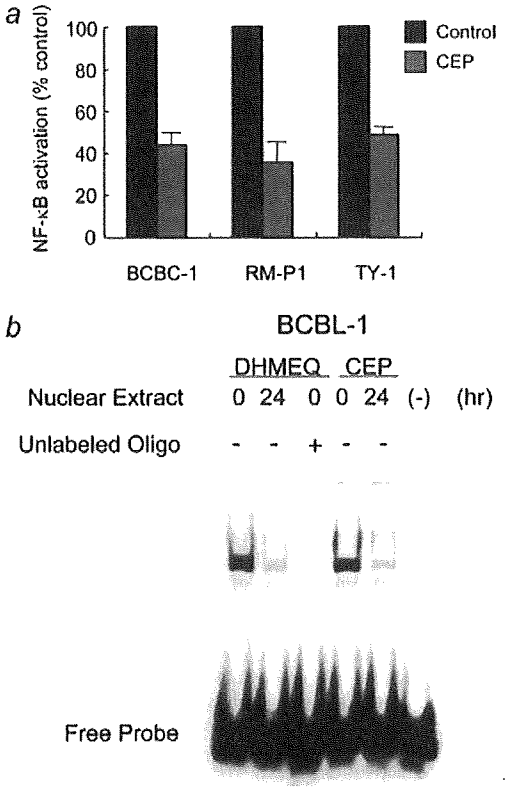

FIGURE 6 – Inhibition of NF-κB activation with CEP. (*a*) The PEL cell lines BCBL-1, TY-1 and RM-P1 were treated with CEP (10 μg/ml) for 24 hr and nuclear proteins were extracted and NF-κB activity was measured by ELISA. Data are expressed as a percentage of control. (*b*) BCBL-1 cells were treated with a specific NF-κB inhibitor, DHMEQ (10 μM) or CEP (10 μg/ml) for 24 hr and assessed for NF-κB DNA binding activity by EMSA using an NF-κB specific oligonucleotide probe. Shown as the mean ± S.D. from 3 independent experiments.

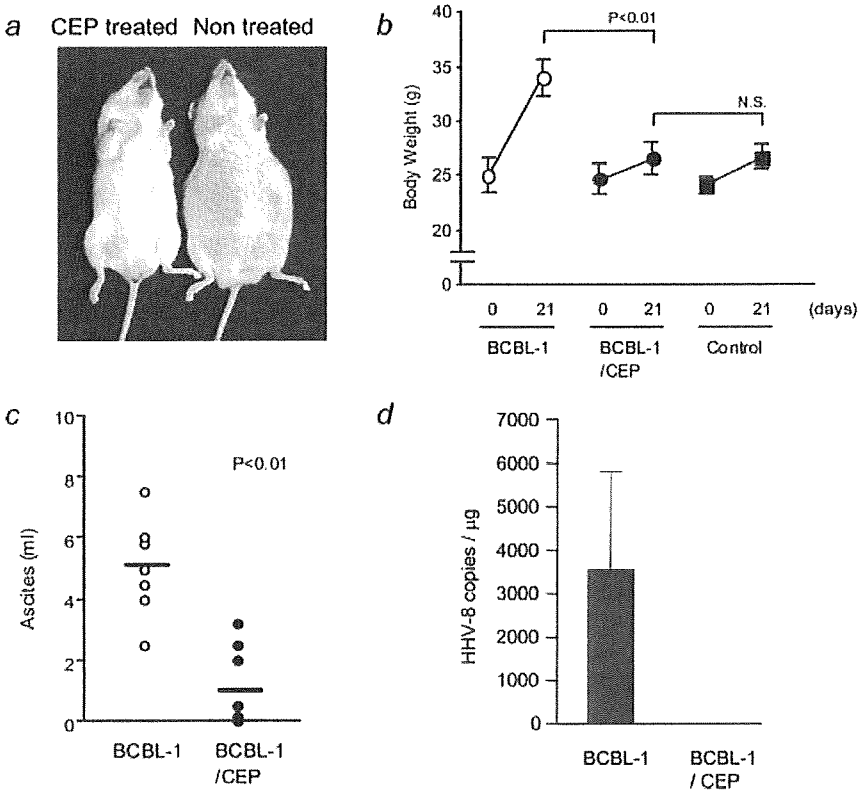

FIGURE 7 – Treatment of NOD/Scid/Jak3 deficient mice with CEP suppresses the development of KSHV-associated lymphoma *in vivo*. (*a*) A photograph of CEP-treated and nontreated ascites-bearing mice 3 weeks after being inoculated with BCBL-1 intraperitoneally. (*b*) The body weight of the mice inoculated with BCBL-1 cells and treated or untreated with CEP, shown as the mean ± S.D. from 7 mice. (*c*) The volume of ascites in mice inoculated with BCBL-1 cells and treated or untreated with CEP, shown as the mean ± S.D. from 7 mice. (*d*) Real-time PCR for KSHV genome. DNA was extracted from the lung, liver and spleen of CEP-treated and untreated mice. Copy number of KSHV ORF26 was measured with a Taqman real-time PCR. [Color figure can be viewed in the online issue, which is available at www.interscience.wiley.com.]

CEP efficiently blocks the constitutive NF-κB activity of PEL cell lines

Several reports have suggested that NF-κB can act as a survival factor and is required for the proliferation of PEL cells.[5,11,38] Because NF-κB is constitutively active in PEL cells,[9] we examined whether CEP inhibits NF-κB activation. When PEL cell lines were treated with 10 μg/ml CEP for 24 hr, the amount of phosphorylated p65 NF-κB protein was severely reduced; however, the amount of p65 NF-κB protein was rather increased, indicating that CEP suppresses NF-κB activity by suppressing the activation of p65 NF-κB (Fig. 5*a*). Suppression of p65 NF-κB activation blocks the nuclear translocation leads to the accumulation of p65 NF-κB protein. Untreated PEL cell lines constitutively expressed both total and phosphorylated IκB, the upstream of NF-κB. CEP treatment slightly reduced phosphorylated IκB and phosphorylated IKKα/β whereas total IκB was slightly increased, suggesting that inhibition of phosphorylation of IκB leads to stabilization of IκB by blocking degradation of IκB protein. Thus, CEP mainly inhibits the p65 NF-κB activation. Next, We fractioned nuclear protein and analyzed the expression of p65 by Western blotting (Fig. 5*b*) to confirm the p65 NF-κB suppression by CEP. When PEL cell lines were treated with 10 μg/ml CEP for 24 hr, the amount of nuclear p65 NF-κB protein was reduced as expected, indicating CEP suppresses NF-κB activity. To confirm that CEP could inhibit NF-κB activity in PEL cell lines, we measured the active NF-κB of nuclear extract by ELISA, and performed an EMSA with DIG labeled double-stranded NF-κB oligonucleotides (Fig. 6). Treatment with CEP suppressed the NF-κB activity in all cell lines tested (Fig. 6*a*). Treatment with DHMEQ, an NF-κB inhibitor, at a concentration of 10 μg/ml abrogated the constitutive NF-κB binding activity in BCBL-1 cells. CEP also abrogated the constitutive NF-κB binding activity (Fig. 6*b*). These results reveal that CEP blocks the constitutive NF-κB activity of PEL cells.

In vivo *effects of CEP on immunodeficient mice that had been inoculated with a PEL cell line*

As the above results suggested the efficacy of CEP for the treatment of PEL patients, we next examined the *in vivo* effects of CEP in an immunodeficient mice model. Severe immunodeficient, NOD/Scid/Jak3 deficient mice (NOJ mice)[33] were inoculated intraperitoneally with 7×10^6 BCBL-1 cells. BCBL-1 produced massive ascites within 3 weeks of inoculation (Fig. 7*a*), and body weight was significantly increased in all mice (Fig. 7*b*). As PEL is characterized by lymphomatous effusions of serous cavities and rarely presents with a definable tumor mass,[1,2] these mice are a clinically relevant PEL model. A dose of 10 mg/kg CEP in PBS or PBS alone was administrated *via* intraperitoneal injection on day 3 after cell inoculation and everyday thereafter for 21 days. CEP treated mice appeared to be healthy, with the same body weight as the nontumor inoculated mice and had a significantly lower volume of ascites (5.2 ± 1.5 ml *vs.* 1.1 ± 1.2 ml, $n = 7$ each, $p < 0.001$) (Fig. 7*b*).The body weight of the nontreated mice was significantly increased compared to that of the CEP treated mice (34.2 ± 1.7 g *vs.* 26.6 ± 1.4 g, $n = 7$, $p < 0.001$; Fig. 7*c*). DNA was extracted from the lung, liver and spleen of CEP-treated and

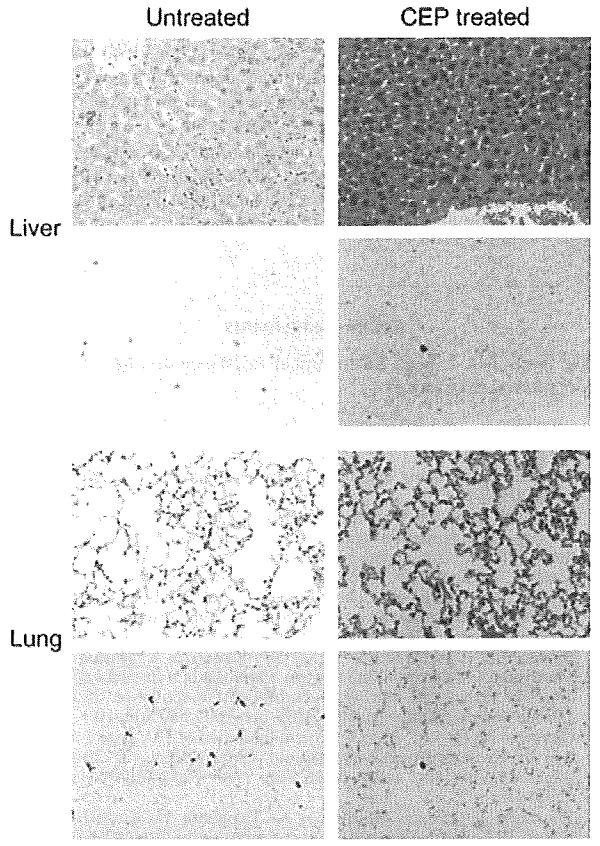

FIGURE 8 – Metastasis of PEL cells into the liver and lungs of the BCBL-1 inoculated mice. Hematoxylin–eosin staining and immunohistochemical staining using anti-LANA (PA1-73N antibody) was performed to detect BCBL-1.

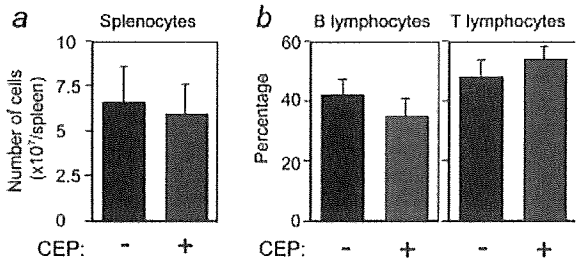

FIGURE 9 – CEP has no adverse effects for murine splenic lymphocytes. (*a*) Number of splenocytes after CEP treatment for 21 days, shown as the mean ± S.D. from 4 mice ($p > 0.05$). (*b*) Percentage of B lymphocytes ($CD19^+$) and T lymphocytes ($CD19^+$) in splenocytes after CEP treatment for 21 days, shown as the mean ± S.D. from 4 mice ($p > 0.05$).

untreated mice. Copy number of KSHV ORF26 revealed that CEP treatment suppressed metastasis (Fig. 7*d*).

Organ infiltration by tumor cells was analyzed and evaluated by Hematoxylin–eosin staining, and LANA immunostaining (Fig. 8). We found that mice inoculated intraperitoneally with BCBL-1 exhibited infiltration into the lung and liver without macroscopic lymphoma formation (Fig. 8). The number of LANA positive cells in CEP treated mice was significantly reduced (0–1cells per field magnification, ×40) compared to the nontreated mice (10–20 cells per field magnification, ×40). These data indicate that CEP significantly inhibits the growth and infiltration of PEL cells *in vivo*.

To investigate the adverse effect of CEP for lymphocytes, a dose of 10 mg/kg CEP in PBS or PBS alone was administrated into Balb/c mice *via* intraperitoneal for 21 days. At the time of sacrifice, the gross anatomical changes were not observed in CEP treated mice including the size of spleen. As shown in Figure 9*a*, the number of splenocytes were not significantly different between CEP treated and untreated mice. Percentages of B lymphocytes and T lymphocytes were also not significantly different (Fig. 9*b*), indicating that there are no significant adverse effects of CEP including for lymphocytes.

Discussion

In the present study, we investigated the direct effects of the biscoclaurine alkaloid CEP on PEL cells *in vitro* and *in vivo*. Our results show that CEP exhibits potent proapoptotic effects on PEL cells and provides evidence that such apoptosis occurs *via* inhibition of NF-κB activity. The rapid and efficient engraftment of PEL cells in NOD/Scid/Jak-3 deficient (NOJ) mice displays characteristics of the human disease and this small animal system is an important step towards developing an *in vivo* model for studying PEL and HHV-8 pathogenesis. Immunodeficient NOD/Scid mice have been previously used as the recipient of human tumor xenograft especially for hematological malignancies,[39,40] as they exhibit complete deficiencies in mature T and B lymphocytes and complement protein, and partial deficiencies in NK cells, macrophages and dendritic cell function.[41,42] Recent advances suggest that complete deficiency of NK cells allows more efficient engraftment of human tumor cells and human hematopoietic stem cells.[43–45] The NOJ mice display a complete deficiency of NK cells like the NOD/Scid/common γ deficient (NOG) mice and provide the ideal microenvironment for the propagation and expansion of PEL cells. The formation of malignant ascites without solid lymphoma formation displayed in PEL xenografted NOJ mice resembles the diffuse nature of human PEL.[1,2]

PEL is an incurable, aggressive B-cell malignancy and most of the patients that suffer from it respond poorly to traditional chemotherapy and develop chemoresistance.[1,2] Several agents have been tested in the search for a more effective treatment for PEL. It is now postulated that the mechanisms of lymphomagenesis involve deregulation of several signaling pathways that may act either independently or crosstalk with each other. These include NF-κB, JAK/STAT and PI3 kinase[4–6] in the case of PEL. PEL is associated with KSHV/HHV-8 infection and KSHV/HHV-8 contains a homologue of the cellular FLIP protein vFLIP, which has the ability to activate the NK-κB pathway.[7,38,46] Moreover, inhibition of NK-κB activity leads to apoptosis of KSHV-infected PEL cells.[5,11] These results suggest that inhibition of NK-κB is an effective target for the treatment of PEL. Activation of NK-κB is involved in various kinds of cancer development and progression[47–49] as well as in virus associated lymphomas,[9] indicating that NF-κB is the good molecular target for cancer treatment.[50]

CEP is one of the biscoclaurine alkaloids that is widely used for the treatment of many acute and chronic diseases in Japan. Antitumor effects and induction of apoptosis by CEP have been reported in the last 10 years.[17–21] Recently, CEP has been shown to inhibit the activation of NF-κB;[12,22,23,51] however, the mechanisms are largely unknown. In our study, we demonstrated that CEP is able to suppress the growth of PEL cells and induce apoptosis *via* the inhibition of NF-κB activity especially by blocking the phosphorylation of p65 NF-κB (Fig. 5*a*). KSHV vFLIP binds to the IKK complex to induce constitutive kinase activation.[10] Consequently, PEL cells have high levels of nuclear NF-κB activity, which is necessary for the survival of PEL cells.[9] Treatment of PEL cells with CEP abrogates the NF-κB activity by blocking phosphorylation of NF-κB p65 (Fig. 5*a*), inhibiting NF-κB nuclear translocation (Fig. 5*b*) and DNA binding activity (Fig. 6*b*). However, as

CEP may not affect KSHV vFLIP, vFLIP continuously activates IKK and results in the retention and accumulation of nonactivated NF-κB p65 (Fig. 5*a*).

CEP has been shown to protect human lymphocytes against radiation-induced apoptosis[52] and oxidative damage.[53] In addition, CEP has been used in Japan for a long time[12] and has shown few side effects,[54–56] and a pharmacokinetic study did not show any adverse effects in volunteer subjects.[57] In this study, we observed administration of CEP showed no significant adverse effects for Balb/C mice (Fig. 8). Moreover, Kikukawa *et al.* recently showed that CEP treatment was effective for the patient with chemotherapy resistant multiple myeloma without obvious side effects.[58] Taken together, CEP is the very useful for the treatment of patients with PEL without side effects. However, the effects of CEP on PEL cells other than NF-κB pathway are still unclear because CEP exerts diverse pharmacological effects.[12] There may be other pathways for inducing the apoptosis of PEL cells other than *via* inhibition of NF-κB. Indeed, CEP has been shown to have a multidrug resistant-reversing effect,[12] to induce cell cycle regulators such as p27Kip1 and p21WAF1,[59] and to activate JNK1/2.[21] Further investigations aimed at determining the efficacy of CEP are warranted and may lead to the development of new effective therapies for this intractable lymphoma.

In conclusion, we have shown the ability of CEP to induce cell death through blocking the NF-κB pathway in PEL cells. Our study provides the rationale for a clinical trial of CEP in patients with PEL and other NF-κB activated tumors.

Acknowledgements

We thank Ms. I. Suzu for technical assistance and Ms. Y. Endo for secretarial assistance.

References

1. Nador RG, Cesarman E, Chadburn A, Dawson DB, Ansari MQ, Sald J, Knowles DM. Primary effusion lymphoma: a distinct clinicopathologic entity associated with the Kaposi's sarcoma-associated herpes virus. Blood 1996;88:645–56.
2. Chen YB, Rahemtullah A, Hochberg E. Primary effusion lymphoma. Oncologist 2007;12:569–76.
3. Cesarman E, Chang Y, Moore PS, Said JW, Knowles DM. Kaposi's sarcoma-associated herpesvirus-like DNA sequences in AIDS-related body-cavity-based lymphomas. N Engl J Med 1995;332:1186–91.
4. Aoki Y, Feldman GM, Tosato G. Inhibition of STAT3 signaling induces apoptosis and decreases survivin expression in primary effusion lymphoma. Blood 2003;101:1535–42.
5. Keller SA, Schattner EJ, Cesarman E. Inhibition of NF-κB induces apoptosis of KSHV-infected primary effusion lymphoma cells. Blood 2000;96:2537–42.
6. Uddin S, Hussain AR, Al-Hussein KA, Manogaran PS, Wickrema A, Gutierrez MI, Bhatia KG. Inhibition of phosphatidylinositol 3′-kinase/AKT signaling promotes apoptosis of primary effusion lymphoma cells. Clin Cancer Res 2005;11:3102–8.
7. Sun Q, Matta H, Chaudhary PM. The human herpes virus 8-encoded viral FLICE inhibitory protein protects against growth factor withdrawal-induced apoptosis via NF-κ B activation. Blood 2003;101: 1956–61.
8. Jarviluoma A, Ojala PM. Cell signaling pathways engaged by KSHV. Biochim Biophys Acta 2006;1766:140–58.
9. Jost PJ, Ruland J. Aberrant NF-κB signaling in lymphoma: mechanisms, consequences, and therapeutic implications. Blood 2007;109: 2700–7.
10. Liu L, Eby MT, Rathore N, Sinha SK, Kumar A, Chaudhary PM. The human herpes virus 8-encoded viral FLICE inhibitory protein physically associates with and persistently activates the Ikappa B kinase complex. J Biol Chem 2002;277:13745–51.
11. Keller SA, Hernandez-Hopkins D, Vider J, Ponomarev V, Hyjek E, Schattner EJ, Cesarman E. NF-κB is essential for the progression of KSHV- and EBV-infected lymphomas in vivo. Blood 2006;107: 3295–302.
12. Furusawa S, Wu J. The effects of biscoclaurine alkaloid cepharanthine on mammalian cells: implications for cancer, shock, and inflammatory diseases. Life Sci 2007;80:1073–9.
13. Shiraishi N, Arima T, Aono K, Inouye B, Morimoto Y, Utsumi K. Inhibition by biscoclaurine alkaloid of lipid peroxidation in biological membranes. Physiol Chem Phys 1980;12:299–305.
14. Nagano M, Kanno T, Fujita H, Muranaka S, Fujiwara T, Utsumi K. Cepharanthine, an anti-inflammatory drug, suppresses mitochondrial membrane permeability transition. Physiol Chem Phys Med NMR 2003;35:131–43.
15. Kondo Y, Imai Y, Hojo H, Hashimoto Y, Nozoe S. Selective inhibition of T-cell-dependent immune responses by bisbenzylisoquinoline alkaloids in vivo. Int J Immunopharmacol 1992;14:1181–6.
16. Goto M, Zeller WP, Hurley RM. Cepharanthine (biscoclaurine alkaloid) treatment in endotoxic shock of suckling rats. J Pharm Pharmacol 1991;43:589–91.
17. Wu J, Suzuki H, Zhou YW, Liu W, Yoshihara M, Kato M, Akhand AA, Hayakawa A, Takeuchi K, Hossain K, Kurosawa M, Nakashima I. Cepharanthine activates caspases and induces apoptosis in Jurkat and K562 human leukemia cell lines. J Cell Biochem 2001;82:200–14.
18. Furusawa S, Wu J, Fujimura T, Nakano S, Nemoto S, Takayanagi M, Sasaki K, Takayanagi Y. Cepharanthine inhibits proliferation of cancer cells by inducing apoptosis. Methods Find Exp Clin Pharmacol 1998;20:87–97.
19. Harada K, Bando T, Yoshida H, Sato M. Characteristics of antitumour activity of cepharanthin against a human adenosquamous cell carcinoma cell line. Oral Oncol 2001;37:643–51.
20. Kono K, Takahashi JA, Ueba T, Mori H, Hashimoto N, Fukumoto M. Effects of combination chemotherapy with biscoclaurine-derived alkaloid (Cepharanthine) and nimustine hydrochloride on malignant glioma cell lines. J Neurooncol 2002;56:101–8.
21. Biswas KK, Tancharoen S, Sarker KP, Kawahara K, Hashiguchi T, Maruyama I. Cepharanthine triggers apoptosis in a human hepatocellular carcinoma cell line (HuH-7) through the activation of JNK1/2 and the downregulation of Akt. FEBS Lett 2006;580:703–10.
22. Okamoto M, Ono M, Baba M. Potent inhibition of HIV type 1 replication by an antiinflammatory alkaloid, cepharanthine, in chronically infected monocytic cells. AIDS Res Hum Retroviruses 1998;14: 1239–45.
23. Tamatani T, Azuma M, Motegi K, Takamaru N, Kawashima Y, Bando T. Cepharanthin-enhanced radiosensitivity through the inhibition of radiation-induced nuclear factor-κB activity in human oral squamous cell carcinoma cells. Int J Oncol 2007;31:761–8.
24. Renne R, Zhong W, Herndier B, McGrath M, Abbey N, Kedes D, Ganem D. Lytic growth of Kaposi's sarcoma-associated herpesvirus (human herpesvirus 8) in culture. Nat Med 1996;2:342–6.
25. Katano H, Hoshino Y, Morishita Y, Nakamura T, Satoh H, Iwamoto A, Herndier B, Mori S. Establishing and characterizing a CD30-positive cell line harboring HHV-8 from a primary effusion lymphoma. J Med Virol 1999;58:394–401.
26. Miyagi J, Masuda M, Takasu N, Nagasaki A, Shinjyo T, Uezato H, Kakazu N, Tanaka Y. Establishment of a primary effusion lymphoma cell line (RM-P1) and in vivo growth system using SCID mice. Int J Hematol 2002;76:165–72.
27. Umezawa K, Ariga A, Matsumoto N. Naturally occurring and synthetic inhibitors of NF-κB functions. Anticancer Drug Des 2000;15: 239–44.
28. Nicoletti I, Migliorati G, Pagliacci MC, Grignani F, Riccardi C. A rapid and simple method for measuring thymocyte apoptosis by propidium iodide staining and flow cytometry. J Immunol Methods 1991;139:271–9.
29. Komoriya A, Packard BZ, Brown MJ, Wu ML, Henkart PA. Assessment of caspase activities in intact apoptotic thymocytes using cell-permeable fluorogenic caspase substrates. J Exp Med 2000;191:1819–28.
30. Ohsugi T, Horie R, Kumasaka T, Ishida A, Ishida T, Yamaguchi K, Watanabe T, Umezawa K, Urano T. In vivo antitumor activity of the NF-κB inhibitor dehydroxymethylepoxyquinomicin in a mouse model of adult T-cell leukemia. Carcinogenesis 2005;26:1382–8.
31. Ohsugi T, Kumasaka T, Ishida A, Ishida T, Horie R, Watanabe T, Umezawa K, Yamaguchi K. In vitro and in vivo antitumor activity of the NF-kappaB inhibitor DHMEQ in the human T-cell leukemia virus type I-infected cell line. HUT-102. Leuk Res 2006;30:90–7.
32. Park SY, Saijo K, Takahashi T, Osawa M, Arase H, Hirayama N, Miyake K, Nakauchi H, Shirasawa T, Saito T. Developmental defects of lymphoid cells in Jak3 kinase-deficient mice. Immunity 1995;3: 771–82.
33. Okada S, Harada H, Ito T, Saito T, Suzu S. Early development of human hematopoietic and acquired immune systems in new born NOD/Scid/Jak3(null) mice intrahepatic engrafted with cord blood-derived CD34 (+) cells. Int J Hematol 2008;88:476–82.